creative commons
COMMONS DEED

저작자표시-비영리-변경금지 2.0 대한민국

이용자는 아래의 조건을 따르는 경우에 한하여 자유롭게

- 이 저작물을 복제, 배포, 전송, 전시, 공연 및 방송할 수 있습니다.

다음과 같은 조건을 따라야 합니다:

저작자표시. 귀하는 원저작자를 표시하여야 합니다.

비영리. 귀하는 이 저작물을 영리 목적으로 이용할 수 없습니다.

변경금지. 귀하는 이 저작물을 개작, 변형 또는 가공할 수 없습니다.

- 귀하는, 이 저작물의 재이용이나 배포의 경우, 이 저작물에 적용된 이용허락조건을 명확하게 나타내어야 합니다.
- 저작권자로부터 별도의 허가를 받으면 이러한 조건들은 적용되지 않습니다.

저작권법에 따른 이용자의 권리는 위의 내용에 의하여 영향을 받지 않습니다.

이것은 이용허락규약(Legal Code)을 이해하기 쉽게 요약한 것입니다.

Disclaimer

dCollection

공학석사 학위논문

Determination of the Longitudinal Dispersion Coefficient in 2D Flows with Submerged Vegetation

침수식생이 있는 2차원 흐름에서의 종방향 분산계수 산정

2013 년 2 월

서울대학교 대학원

건설환경공학부

박 선 영

Determination of the Longitudinal Dispersion Coefficient in 2D Flows with Submerged Vegetation

침수식생이 있는 2차원 흐름에서의 종방향 분산계수 산정

지도교수 서 일 원

이 논문을 공학석사 학위논문으로 제출함
2012 년 10 월

서울대학교 대학원
건설환경공학부
박 선 영

박선영의 공학석사 학위논문으로 인준함
2012 년 12 월

위 원 장 _____ (인)

부위원장 _____ (인)

위 원 _____ (인)

ABSTRACT

Determination of the Longitudinal Dispersion Coefficient in 2D Flows with Submerged Vegetation

Sun Young Park
Department of Civil and Environmental Engineering
Seoul National University

The transport processes in the riparian environment is a subject of great interest. Vegetation plays a key role in the sustainable development of the aquatic environment by strongly influencing both water conveyance and mass transport.

Prior to determination of the longitudinal dispersion coefficient, the study carried out the derivation and investigation of a theoretical solution for the combined wave-current flow through submerged vegetation. A depthwise logarithmic velocity profile was assumed to formulate the current in the overflow region with a virtual bottom boundary near the interface which becomes depthwise constant in the vegetation region. To induce the wave element, small-amplitude waves were assumed and using a linear wave theory, the wave components were derived to the first order for both of the velocities. Stream functions for combined flows were obtained separately for overflow

and vegetation regions and then coupled at interface to find expressions for monami (aquatic plant wave).

The two-box model adopted from Murphy et al. (2007) was modified composing of the longitudinal dispersion terms in each adjusted region. For larger submergence depth the LDC gradually approached to the value of a simple analytical expression regardless of vegetation. Consideration of the flexibility formulated by wave motion resulted in differences between total LDCs about 25% at relatively small submergence depth. The steady part showed a more significant role at large time on the LDC than the periodic part. This meant for long period wave, the concentration can adopt the velocity profile of itself. Therefore the LDC will be the same as if flow were steady except during a short period.

keywords: submerged vegetation, flexibility, longitudinal dispersion, K-H instability, monami, two-box model

Student Number: 2011-20975

TABLE OF CONTENTS

ABSTRACT ..... **iii**

TABLE OF CONTENTS ..... **v**

LIST OF FIGURES ..... **vii**

LIST OF TABLES ..... **viii**

LIST OF SYMBOLS ..... **ix**

1. Introduction **14**

1.1 Background 14

1.2 State of the art review 15

1.3 Objective 21

2. Theoretical Background **23**

2.1 Longitudinal dispersion 23

2.1.1 *N*-zone method 23

2.1.2 Two-box model 27

2.2 Characteristics of flows through vegetation 32

2.2.1 Submergence 34

2.2.2 Flexibility 39

2.2.3 Monami of interface 41

3. Velocity Profile **46**

3.1 Overflow region 49

3.1.1 Governing equations 52

3.1.2 Boundary conditions 53
3.1.3 Stream function of overflow region 55
3.1.4 The first order solution 56
3.2 Vegetation region 64
4. Longitudinal Dispersion Coefficient 71
4.1 Modified Two-box model 71
4.1.1 Vortex-driven exchange 71
4.1.2 Diffusion-limited exchange 74
4.2 Determination of longitudinal dispersion coefficient 75
5. Results and Conclusion 82
5.1 Results 82
5.2 Conclusion 87
6. Reference 90

LIST OF FIGURES

Figure 1.1 Aquatic environment 16

Figure 1.2 Velocity profile in and above a submerged canopy.....19

Figure 1.3 Effects of wave motion due to flexibility 22

Figure 2.1 *N*-zone model for open-channel flow.....25

Figure 2.2 Concentration profile and mean gradients in the *N*-zone model....25

Figure 2.3 Two-zone model for flows with submerged canopies.....28

Figure 2.4 Factors of flows through vegetation 33

Figure 2.5 Three regimes of canopy flow 35

Figure 2.6 Scheme of Kelvin–Helmholtz instabilities 36

Figure 2.7 Configurations of flexible vegetation 40

Figure 2.8 Experimental configuration and the eelgrass meadow 44

Figure 3.1 Schematic diagram of wave-current flow.....47

Figure 3.2 Overflow region.....50

Figure 3.3 Vector diagrams of submergence depth, $H / h = 3$ 63

Figure 3.4 Vector diagrams of submergence depth , $H / h = 12$ 63

Figure 3.5 Vegetation region 65

Figure 5.1 Contributions of each term to dispersion coefficient.....83

Figure 5.2 Difference of each exchange terms.....84

Figure 5.3 Variation of the LDC for two extremities 86

LIST OF TABLES

Table 1.1 Overview of the velocity profiles for submerged vegetation 17

Table 2.1 Comparison of frequencies.....45

Table 4.1 Differences between two models.....72

LIST OF SYMBOLS

Latin Uppercase

$A_n(z_0)$	Fourier coefficients of z_0 $(n=0,1)$
$A_{nv}(z)$	Fourier coefficients of z_0 $(n=0,1)$
B_n	integration constants $(n=1,2)$
C_1	concentration of overflow region
C_2	concentration of vegetation region
C_D	drag coefficient for the vegetation
C_j	concentration of jth layer $(j=1, 2, \ldots, N)$
C_u	coefficient for overflow region
D	diffusion coefficient
$D(N)$	longitudinal dispersion of N zone
D_v	turbulent diffusion coefficient
D_w	wake-zone diffusion coefficient
D_{xj}	average longitudinal diffusivity $(j=1, 2, \ldots, N)$
$D_{zj(j+1)}$	average vertical diffusivity $(j=1, 2, \ldots, N-1)$
H	water depth
I_o	shear term of overflow
K_1	longitudinal dispersion of overflow region $(=K_o)$
K_2	longitudinal dispersion of vegetation region $(=K_v)$
K_d	stem-related dispersion

K_{ss}	longitudinal dispersion for submerged stiff vegetation case
K_{sf}	longitudinal dispersion for submerged flexible vegetation case
K_{vs}	dispersion of emergent vegetation
K_{wx}	longitudinal dispersion in wave-current flow
L	wave length
N	number of vegetation per unit area
S	channel slope
S_b	surface energy gradient
$S(x, z_0, t)$	free surface
T	wave period
U	instantaneous velocity in *x* direction
$U(x)$	depth and period-average velocity
U_1	mean velocity of overflow region ($=U_o$)
U_2	mean velocity of overflow region ($=U_v$)
U_c	steady current velocity
U_j	average velocity of jth layer ($j = 1, 2, \ldots, N$)
U_{oc}	steady current velocity of overflow region
U_{ow}	first-order wave-induced velocity of overflow region
U_w	first-order wave-induced velocity
V	instantaneous velocity in *y* direction
$\mathbf{V}$	velocity vector ($=\partial\psi_1/\partial z_0\mathbf{i} - \partial\psi_1/\partial x\mathbf{j}$)
W	instantaneous velocity in *z* direction

Latin Lowercase

a	surface wave amplitude
a_n	Fourier coefficient for wave
b	exchange coefficient
c	celerity ($=\sigma / k$)
d	stem diameter
g	gravitational acceleration
h	height of vegetation
h_1	water depth of overflow region for submerged stiff vegetation case
h_2	water depth of vegetation region for submerged stiff vegetation case
h_d	deflected height of flexible vegetation
h_j	water depth of jth layer ($j = 1, 2, \ldots, N$)
h_o	water depth of overflow region for submerged flexible vegetation case
h_v	water depth of vegetation region for submerged flexible vegetation case
i	energy gradient
k	exchange velocity ($=\Delta U / 40$); wave number
m	stem density
p	pressure
q_j	fraction of h_j ($= h_j / H$)
s	separation individual elements

u_1	logarithmic velocity of current part for overflow region
u_2	depthwise constant velocity of current part for vegetation region
u_*	shear velocity
y'	displacement of plant
$z*$	physical vertical coordinate
w_1	vertical velocity for overflow region
w_2	vertical velocity for vegetation region
z_0	new origin shifted from its original location of channel bottom
z_1	elevation of virtual bed

Greek Lowercase

α	constant (= $40\alpha_1^2\alpha_2$)
α_1	constant fraction (= $U_o - U_v / \Delta U$)
α_2	constant (= $\Delta U / u_*$)
β_1	constant of wave part for overflow region
β_2	constant of wave part for vegetation region
η_1	periodic disturbance on the free surface
η_2	periodic disturbance at the interface
κ	von Karman constant
ξ	moving coordinate of space

ρ	water density
σ	wave frequency
τ	moving coordinate of time
ς	constant (= $4.2[(U_o - U_v) / u_{*H}]^2$)
ψ_1	stream function of overflow region (= ψ_o)
ψ_2	stream function of vegetation region (= ψ_v)
ψ_c	stream function of steady current for overflow region
ψ_{oc}	stream function of steady current for overflow region
ψ_{ow}	stream function of first-order wave motion for overflow region

Special Symbols

∇	2D differential operator
∇^2	2D Laplacian operator

1. Introduction

1.1 Background

Vegetation proliferates floodplains, banks (riparian vegetation), and riverbeds (aquatic vegetation). Presence of the plants in a stream causes mechanical obstruction to the flow by changing velocity fields, and, as a result, vegetation alters the hydraulic regime of a flow, and its transport and mixing processes which are crucial for the fluvial environment. Although the effect of an individual plant on the flow can be very local and relatively minor, communities are capable of generating significant changes in the environment.

Because of the involvement of physical and biological components, the problem of vegetation in streams is complex and requires multidisciplinary approach to be understood and comprehended quantitatively. However, river engineers were concerned mainly with the effects of increased resistance to the flow. The value of understanding of these complex mechanisms is dictated also by the increased demands of various environmental issues and its consequence for the fluvial systems.

1.2 State of the art review

An important velocity profile for emergent vegetation on littoral zone (Figure 1.1) is the equation of Petryk and Bosmaijan (1975). Other descriptions for emergent vegetation and the descriptions for submerged vegetation show resemblance with the equation of Petryk and Bosmaijan, especially for describing the velocity in the vegetation layer. Therefore, it was concluded that further investigation of descriptions for emergent vegetation were not necessary.

For submerged vegetation on limnetic zone (Figure 1.1), most descriptions of the velocity are based on the two layer theory with a distinction between the vegetation layer and the surface layer. For defining the velocity in the vegetation layer (Table 1.1), several different approaches are used. Klopstra et al. (1997) identified with three definitions for the turbulent length scale and Huthoff (2007) defined the velocity in the vegetation layer by considering the influence of the higher velocities in the surface layer. Others, Nepf and Vivoni (2000), Stone and Shen (2002), Van Velzen et al. (2003), Baptist et al. (2006) and Yang and Choi (2010) assume a constant velocity

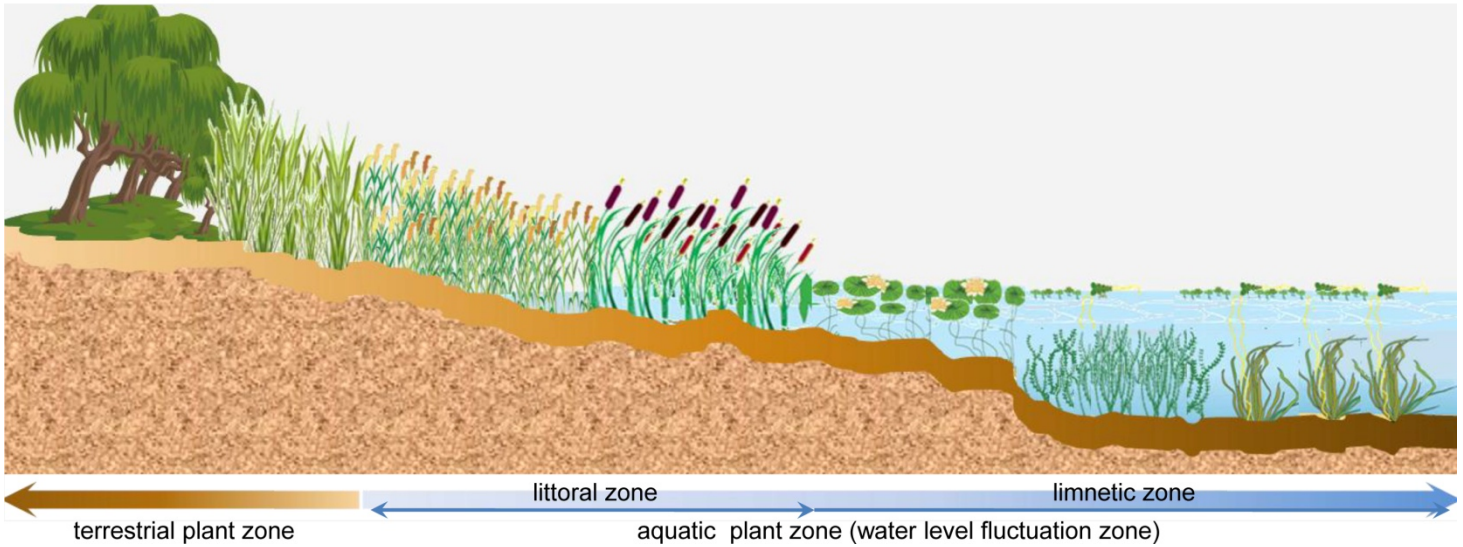

Figure 1.1 Aquatic environment (Lee and Kim, 2005)

Table 1.1 Overview of the velocity profiles for submerged vegetation

Author	Equation	Notation and symbol
Klopstra et al. (1997)	$U = \frac{h \cdot U_v + (H-h) \cdot U_o}{H}$	C_D : drag coefficient C_u : coefficient for overflow region d : diameter of cylindrical elements g : gravitational acceleration h : height of resistance elements H : water depth N : number of cylinders of unit area i : channel slope s : separation individual elements [m] U : depth-averaged velocity [m / s] U_o : depth-averaged velocity in overflow region [m / s] U_v : depth-averaged velocity in vegetation region [m / s] κ : Von Karman's constant (0.41)
Stone and Shen (2002)	$U = \sqrt{\frac{2g}{C_D \cdot d \cdot N}} \sqrt{i} \cdot \left(1 - d\sqrt{N}\right) \cdot \sqrt{\left(\frac{H}{h} - \frac{1}{4}\pi N d^2\right) \cdot \frac{H}{h}}$	
Van Velzen et al. (2003)	$U = \sqrt{\frac{2g}{C_D \cdot d \cdot N}} \sqrt{i} + 18\left(H-h\right)^{3/2} \frac{\sqrt{i}}{h} \cdot \log \frac{12\left(H-h\right)}{1.6 \cdot h^{0.7}}$	
Baptist et al. (2006)	$U = \left(\sqrt{\frac{2g}{C_D \cdot d \cdot N}} \sqrt{i} \cdot \sqrt{h} + \frac{\sqrt{g}}{\kappa} \ln\left(\frac{H}{h}\right) \cdot \sqrt{i} \right) \sqrt{H}$	
Huthoff (2007)	$U = \sqrt{\frac{2g}{C_D \cdot d \cdot N}} \sqrt{i} \cdot \left(\sqrt{\frac{h}{H}} + \frac{H-h}{H} \left(\frac{H-h}{s} \right)^{2/3} \right)$	
Yang and Choi (2010)	$U = \sqrt{\frac{2gh}{C_D \cdot d \cdot N}} \sqrt{i} + \frac{C_u \cdot u_*}{\kappa} \left[\ln \frac{H}{h} - \frac{H-h}{H} \right]$	

over the depth in the vegetation layer. Most of these descriptors define the velocity in the surface layer by a logarithmic profile, except the description of Stone and Shen (2002).

A theoretical description for flexible vegetation with input parameters which can be measured in the field is still lacking. The above mentioned descriptions for rigid vegetation are also used to predict the behavior of flexible vegetation. Therefore, even though its form has been simplified, it is needed to improve understanding of flexible vegetation.

Raupach et al. (1996) concluded that the structure of flow over terrestrial vegetation is better represented by the model analogous to hydrodynamic mixing layer model rather than by a perturbed boundary layer model (Figure 1.2). It was radical and stimulated the deeper understanding of turbulence and its coherent structures. Recently these ideas were fully adopted to the studies of the flows with aquatic vegetation (Nepf and Vivoni 2000; Ghisalberti and Nepf 2002). The velocity profile in the flow with submerged vegetation has a distinctive inflection point which existence is a precondition for generation of the Kelvin-Helmholz instabilities that evolve into the large-scale coherent structures (Ghisalberti and Nepf 2002). Presently this approach

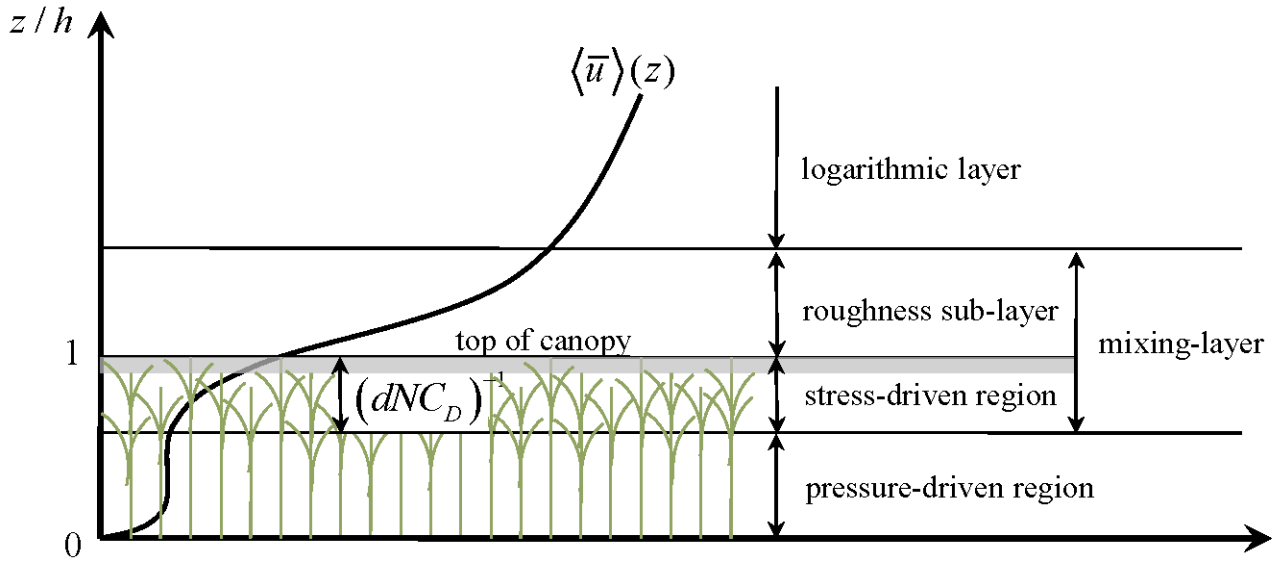

Figure 1.2 Velocity profile in and above a submerged canopy (Gayev and Hunt, 2006)

represents a frontier for many ongoing theoretical and laboratory studies and is intensively exploited and further developed in this study.

With respect to the longitudinal dispersion model, Geoffrey Taylor (1953) introduced the concepts for the first time. Since that time the model was tested in laboratory (Elder 1959) and natural open-channel flows (Fischer, 1973; Seo and Cheong, 1998; Deng et al., 2001; Seo and Baek, 2004). These studies have indicated that the distributions of concentration deviate by the model of longitudinal dispersion. In some cases, differences were shown to the accumulation and the delayed release of the transported substances in non-transit zones of the flow, dead-zones, i.e. regions in the flow field with zero or relatively low longitudinal velocity. The studies of larger scale dead zones, such as bed depression or side arms, have shown that the trapping and delay of some fraction of the particles enhances the longitudinal dispersion, and creates long tails on the distribution of slug releases (Chikwendu, 1986; Seo, 1990; Rutherford, 1994). Recently the dispersion processes attracted attention in respect to the vegetated flows, and the model of longitudinal dispersion with dead zones was applied to interpret the dynamics of transport and mixing processes in wetlands (Nepf, 1999; Murphy et al., 2007).

1.3 Objective

Based on the backgrounds and necessities, derivation of velocity profile which can reflect the effect of flexible vegetation on submerged state is primary with assumption that factor of longitudinal dispersion coefficient is confined only to the velocity profile. The ultimate objective of this study is determination of longitudinal dispersion coefficient theoretically using the solution of the combined wave-current flow (Figure 1.3) through submerged vegetation. The reason this study choose the approach is individual plants are seldom growing alone – more often they form communities called patches. In addition, characteristic of easily bending can show the effect of wave motion, i.e., the combined wave-current flow makes patches lapping within the flow acted as cause and effect.

(a) Velocity profile in flows with submerged vegetation

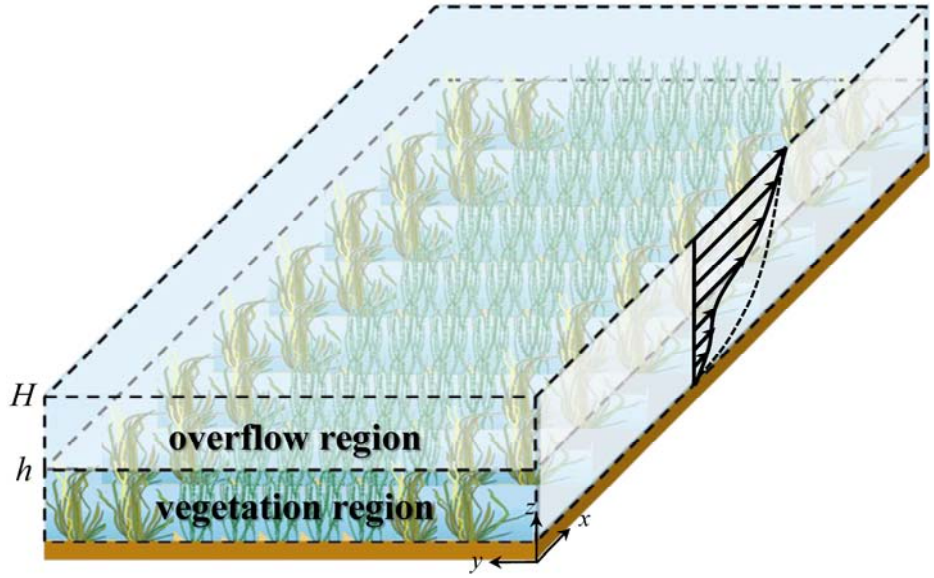

(b) Combined wave-current flow

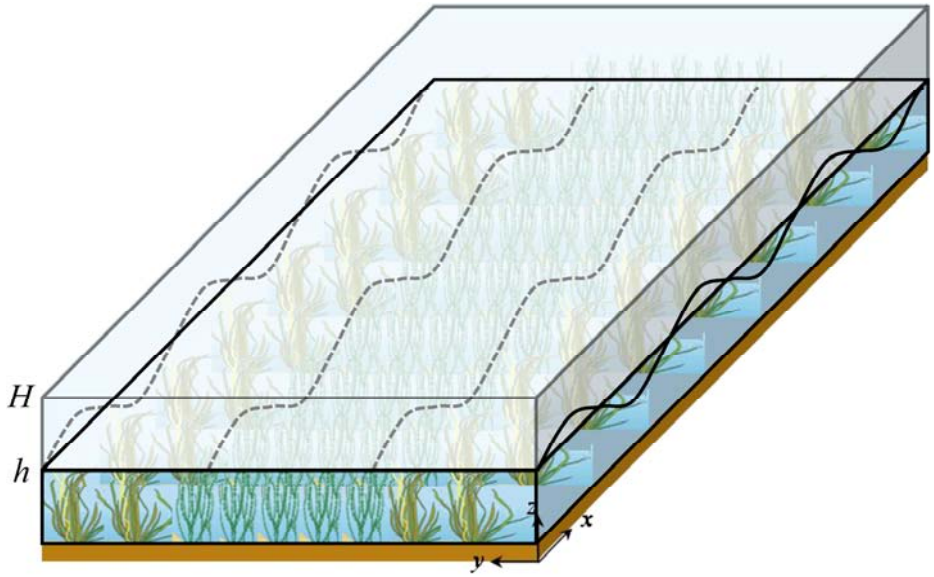

Figure 1.3 Effects of wave motion due to flexibility

2. Theoretical Background

2.1 Longitudinal dispersion

2.1.1 *N*-zone method

Chikwendu (1986) developed a method of zones in which the flow is divided into *N* zones of parallel flow, each of which is considered to be well mixed. A dispersion equation is obtained in each zone and cross-stream mixing between the zones is taken into account, leading to a system of *N* coupled dispersion equations. The exact longitudinal dispersivity at large times is calculated for the *N*-zone model and in the limit as *N* tends to infinity an integral expression is obtained for the dispersivity. This integral expression is in agreement with the formulas of Taylor and Aris and is an exact large-time analytical result.

If the two-dimensional open channel flow is divided into *N* zones of parallel flow with thicknesses h_j, contaminant concentrations C_j , average velocities U_j and average longitudinal diffusivities D_{xj}, respectively, in each

well mixed zone (with j = 1 , 2 , …, N) as shown in Figures 2.1-2.2, then the N coupled dispersion equations are

$$\frac{\partial C_1}{\partial t} + u_1 \frac{\partial C_1}{\partial x} = D_{x1} \frac{\partial^2 C_1}{\partial x^2} + b_{12} q_1 (C_2 - C_1) \tag{2.1a}$$

$$\frac{\partial C_j}{\partial t} + u_j \frac{\partial C_j}{\partial x} = D_{xj} \frac{\partial^2 C_j}{\partial x^2} + b_{(j-1)j} q_j (C_{j-1} - C_j) + b_{j(j+1)} q_j (C_{j+1} - C_j) \tag{2.1b}$$

…

$$\frac{\partial C_N}{\partial t} + u_N \frac{\partial C_N}{\partial x} = D_{xN} \frac{\partial^2 C_N}{\partial x^2} + b_{(N-1)N} q_N (C_{N-1} - C_N) \tag{2.1c}$$

where

$$q_j = \frac{h_j}{H} \quad (j = 1, 2, \ldots, N), \tag{2.2a}$$

$$b_{j(j+1)} = \frac{2 D_{yj(j+1)}}{H^2 (q_j + q_{j+1})} \quad (j = 1, 2, \ldots, N-1), \tag{2.2b}$$

and $D_{yj(j+1)}$ is the average vertical diffusivity between zones j and (j + 1). In order to calculate the zonal longitudinal diffusivities D_{xj}. Chikwendu regards the dispersion process as if it takes place in two-stages following contaminant discharge into the flow.

In the first stage the contaminant mass in each zone disperses exclusively in that zone with no contaminant-mass exchange between the zones. After some time the Taylor asymptotic dispersion stage would be

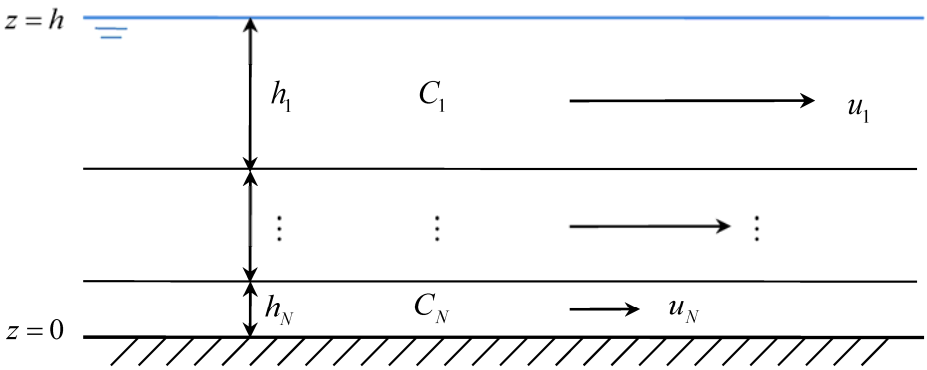

Figure 2.1 *N*-zone model for open-channel flow (Chikwendu, 1986)

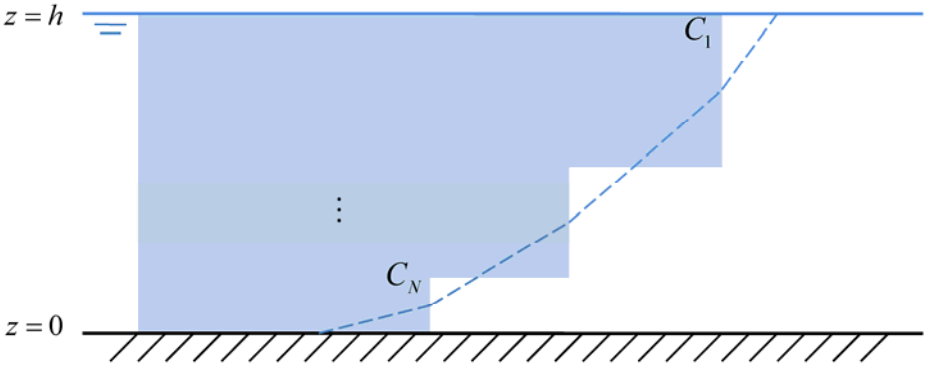

Figure 2.2 Concentration profile and mean gradients in the *N*-zone model (Chikwendu, 1986)

reached in each zone and the governing advective-diffusion equations would be separate one-dimensional dispersion equations in each zone, that is,

$$\frac{\partial C_j}{\partial t} + u_j \frac{\partial C_j}{\partial x} = D_{xj} \frac{\partial^2 C_j}{\partial x^2} \quad (j = 1, 2, \ldots, N). \tag{2.3}$$

Thus D_{xj} is defined as the Taylor longitudinal dispersivity that would be obtained in the jth zone if there were no contaminant mixing between the zones. The solution of Eq. (2.3) would lead to N separate Gaussian clouds moving downstream.

In the second stage of the dispersion process contaminant-mass exchange takes place between the zones. This exchange leads to Eq. (2.1). Thus at large times a single Gaussian cloud is obtained.

In principle the system Eq. (2.1) can be analyzed and be simplified using Fourier transformation with the use of a large-time exponent and the longitudinal dispersion is given by

$$D(N) = \sum_{j=1}^{N-1} \frac{(q_1 + \cdots + q_j)^2 \left[1 - (q_1 + \cdots + q_j)^2\right]^2 \left[u_{12\ldots j} - u_{(j+1)\ldots N}\right]^2}{b_{j(j+1)}} + \sum_{j=1}^{N} q_j D_{xj} \tag{2.4}$$

where

$$u_{12\ldots j} = \left(\sum_{k=1}^{j} q_k u_k \right) \Big/ \left(\sum_{k=1}^{j} q_k \right) \quad = \text{mean velocity in the first j zones} \qquad (2.5a)$$

and

$$u_{(j+1)\ldots N} = \left(\sum_{k=j+1}^{N} q_k u_k \right) \Big/ \left(\sum_{k=j+1}^{N} q_k \right) \quad = \text{mean velocity in the last } (N - j) \text{ zones.} \qquad (2.5b)$$

The discrete *N*-zone model becomes an exact continuum model taking the limit as $N \to \infty$.

2.1.2 Two-box model

This study adopted the two-box model and the conceptual model is shown in Figure 2.3, which shows a two-dimensional (*x* and *z*) flow in an open channel divided into an upper fast zone and a slow zone near the boundary. Constant mean velocities (U_1 and U_2) are assumed for the fast and slow zones, in that order. The two layers are assumed to be well mixed with concentrations C_1 and C_2. The Taylor dispersion coefficients for the layers, K_1 and K_2, are obtained by evaluating for each zone separately. Exchange between the zones is characterized by the exchange coefficient, *b*, with dimensions T^{-1}. Thus, the

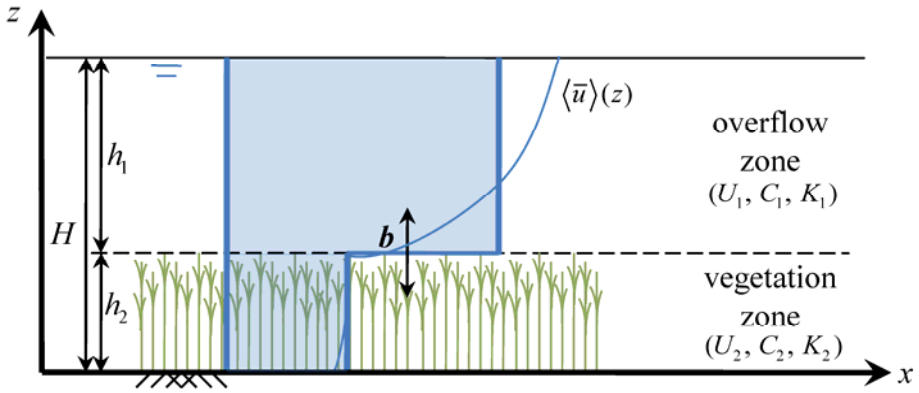

Figure 2.3 Two-zone model for flows with submerged canopies (Murphy et al., 2007)

coupled advection-dispersion equations for each layer are

$$\frac{\partial C_1}{\partial t} + U_1 \frac{\partial C_1}{\partial x} = K_1 \frac{\partial^2 C_1}{\partial x^2} + b\left(\frac{H}{h_1}\right)(C_2 - C_1) \tag{2.6a}$$

$$\frac{\partial C_2}{\partial t} + U_2 \frac{\partial C_2}{\partial x} = K_2 \frac{\partial^2 C_2}{\partial x^2} + b\left(\frac{H}{h_2}\right)(C_1 - C_2) \tag{2.6b}$$

The only difference between these equation and general advection-dispersion equation is the additional coupling term to account for transfer of mass across the boundary of the layers ($z = h_2$). The solution of this set of equations proceeds as follows. The Fourier transforms of $C_1(x,t)$ and $C_2(x,t)$ are defined as

$$\hat{C}_1(k,t) = \int_{-\infty}^{\infty} C_1(x,t) e^{-ikx} dx \tag{2.7a}$$

$$\hat{C}_2(k,t) = \int_{-\infty}^{\infty} C_2(x,t) e^{-ikx} dx \,. \tag{2.7b}$$

Substitution of Eq. (2.7) into the partial differential equations, Eq. (2.6), reduces the problem to a system of ordinary differential equations:

$$\frac{\partial \hat{C}_1}{\partial t} + ikU_1\hat{C}_1 = -k^2 K_1 \hat{C}_1 + b\left(\frac{H}{h_1}\right)(\hat{C}_2 - \hat{C}_1) \tag{2.8a}$$

$$\frac{\partial \hat{C}_2}{\partial t} + ikU_2\hat{C}_2 = -k^2 K_2 \hat{C}_2 + b\left(\frac{H}{h_2}\right)(\hat{C}_1 - \hat{C}_2) \,. \tag{2.8b}$$

Chikwendu and Ojiakor (1985) assumed exponential solutions of the form $\hat{C}_1 = f(k)e^{\gamma(k)t}$ and $\hat{C}_2 = g(k)e^{\gamma(k)t}$, giving a characteristic equation of the

system,

$$\gamma^2 + \gamma\left[ik(U_1 + U_2) + k^2(K_1 + K_2) + bH\left(\frac{1}{h_1} + \frac{1}{h_2}\right)\right]$$
$$+\left[ik^3(U_1K_2 + U_2K_1) + k^2(k^2K_1K_2 - U_1U_2) + ikbH\left(\frac{U_1}{h_2} + \frac{U_2}{h_1}\right)\right] = 0. \quad (2.9)$$

Since this study is only interested in the dispersion coefficient in the Fickian limit as $t \to \infty$, higher order terms in *k* disappear and $\gamma \approx ikB - k^2A$, where *A* and *B* are constants. Then, plug this value for γ back into the expression for $\hat{C}_1$ and $\hat{C}_2$ and taking an initial condition of $\hat{C}_1(k,0) = \hat{C}_2(k,0) = C_0$, invert $\hat{C}_1$ and $\hat{C}_2$ to find that the concentration distributions in two layers are equal at long times and are given by

$$C(x,t) = \frac{C_0}{\sqrt{4\pi At}} \exp\left[\frac{-(x - Bt)^2}{4At}\right]. \quad (2.10)$$

This resembles a Gaussian solution with mean velocity, $B = U = \left(\frac{h_1}{H}\right)U_1 + \left(\frac{h_2}{H}\right)U_2$, and asymptotic dispersion coefficient, $A = K_z$. Chikwendu (1986) determined these constants analytically by substituting γ back into Eq. (2.9) and, setting the coefficients of k^i to zero, for *i* = 0, 1, and 2. This confirms that $B = U$ and yielded a final solution for the longitudinal dispersion coefficient,

$$K_x = \frac{\left(\frac{h_1}{H}\right)^2 \left(\frac{h_2}{H}\right)^2 (U_2 - U_1)^2}{b} + \left(\frac{h_1}{H}\right) K_1 + \left(\frac{h_2}{H}\right) K_2 \quad . \tag{2.11}$$

By definition, the exchange coefficient, b, is the inverse of the time scale for vertical mixing across the two layers. Thus,

$$b^{-1} \simeq \frac{h_2^2}{D_w} + \frac{h_1}{k} + \frac{h_1^2}{\left[\frac{1}{h_1}\int_{h_2}^{H} D_z dz\right]} \tag{2.12}$$

The resulting formula Eq. (2.11) emphasizes the importance in dispersion of the velocity differences (shear) between the fast and slow regions of the flow.

The first and the second term in Eq. (2.12) represent the time scale for turbulent-diffusive transport across the wake zone and the time scale for vortex-driven flushing of the exchange zone, for which Nepf and Ghisalberti (2008) determined the exchange velocity, $k = \Delta U / 40$. Finally, the last term is the time scale for transport across the fast zone.

The second term in Eq. (2.11) contains K_1, which epitomizes the longitudinal dispersion in the fast zone due to large-scale velocity shear in this region. Above the canopy, the velocity profile reverts to a logarithmic profile for $z > h_2$, with a virtual bottom boundary near $z = h_2$ (Nepf and Vivoni, 2000). Thus, Elder's simple analytical expression is expected to hold in the

region $h_2 < z < H$, yielding $K_1 = 5.93u_*(H - h_2) = 5.93u_*h_1$ where $u_* \equiv \sqrt{gS(H - h_v)}$.

The third term in Eq. (2.11) stands for dispersion in the slow zone. K_2 is assumed equivalent to the dispersion coefficient in an emergent canopy and it can be embodied by $K_2 = K_{vs} + K_d$ where K_{vs} and K_d imply the in-canopy vertical shear $K_{vs} = -\frac{1}{H}\int_0^H \langle\bar{u}\rangle'' \int_0^z \frac{1}{D_z}\int_0^z \langle\bar{u}\rangle'' \, dz\, dz\, dz$ and stem-scale contributions to dispersion, respectively, where $\langle\bar{u}(z)\rangle'' = \langle\bar{u}(z)\rangle - U$ and D_z is turbulent diffusion. In sparse canopies (dimensionless density $d^2N < 0.1$, where d is the mean diameter of plans), K_d can be approximated by $K_d = \frac{1}{2}C_D^{1/3}U_1 d$ (Lightbody and Nepf, 2006). Also, White and Nepf (2003) suggested $K_d \cong 5d^2NU_1 d$ for a dense ($d^2N > 0.1$).

2.2 Characteristics of flows through vegetation

Primary factors determining characteristics of vegetated flows are submergence depth (H / h), flexibility, and density (Figure 2.4). The target of this study is flexible vegetation influenced by submergence and density. In this section, former researches about the main factors are described.

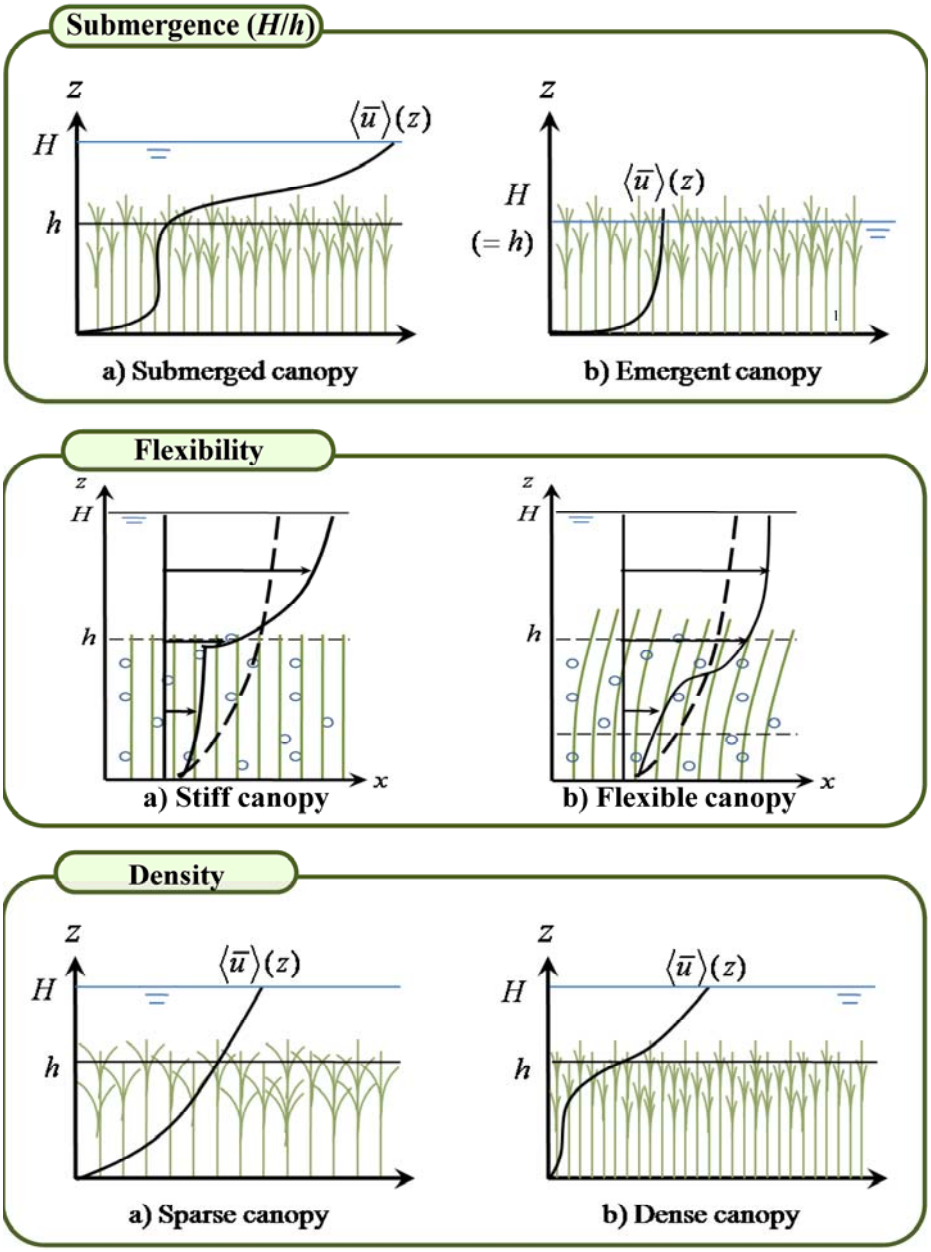

Figure 2.4 Factors of flows through vegetation

2.2.1 Submergence

The range of flow condition observed in aquatic systems is depicted in Figure 2.5. Conditions span from the unconfined canopy, in which the flow depth is much greater than the canopy height, to the emergent canopy, in which the canopy fills the entire flow depth. Unconfined canopy closely resembles terrestrial conditions. The discontinuity in drag at the top of the canopy creates a region of strong shear. This region of the velocity profile resembles a free-shear-layer and includes an inflection point just within the canopy. A free-shear-layer is characterized by large coherent vortices that form via Kelvin-Helmholtz (KH) instability and which dominate the transport across the layer (Aeschlimann, 2012). In terrestrial canopies, these coherent structures have been shown to play an important role in transport between the canopy and overlying atmosphere. Far above the canopy the flow returns to a boundary layer structure. The in-canopy flow is driven by the turbulent stress at the top of the canopy, and it decays with distance from the top of the canopy due to the significant momentum absorption by the canopy. There are three distinct scales of turbulence. The boundary layer

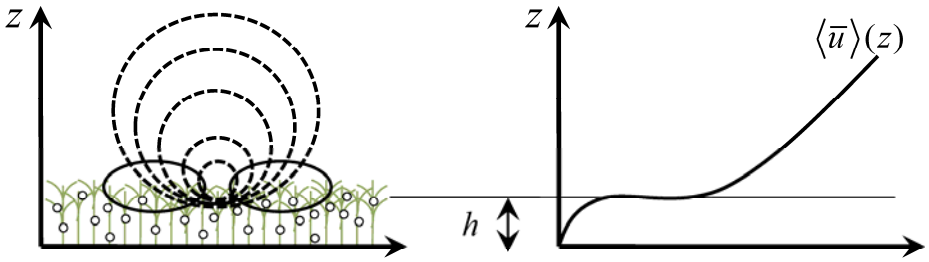

a) unconfined canopy

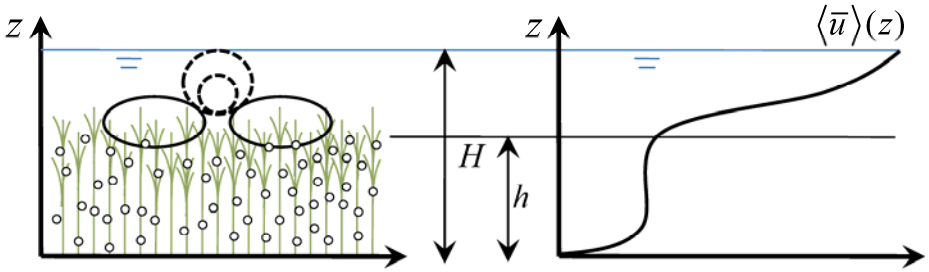

b) submerged canopy

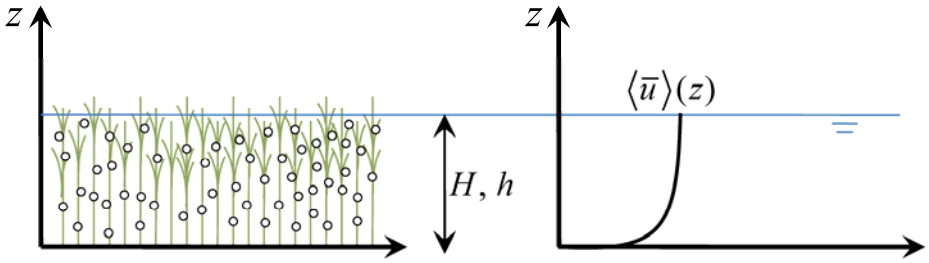

c) emergent canopy

Figure 2.5 Three regimes of canopy flow

(modified from Gayev and Hunt, 2006)

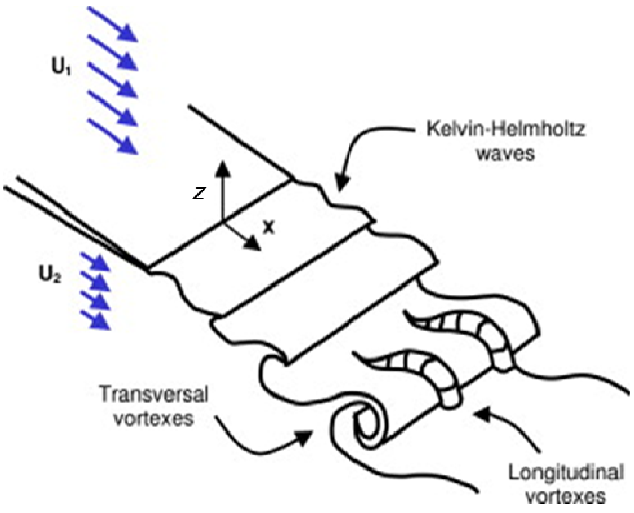

Figure 2.6 Scheme of Kelvin–Helmholtz instabilities (Aeschlimann, 2012)

turbulence (large dashed circles in Figure 2.5) has the largest scale, but contributes little to vertical transport at the canopy interface. The KH vortices at the canopy interface (shown as solid black ovals) have the most impact on vertical transport. Observations in terrestrial canopies has suggested that interaction between the boundary layer and KH eddies causes the KH structures to be intermittent. Finally, the turbulence produced within the canopy at the scale of the canopy elements is too small to contribute to transport, but its production drains energy from both the mean flow and larger turbulent scales.

Aquatic canopies that are deeply submerged have flow structure that is similar to terrestrial canopies, in that a mixing-layer and KH vortices are present at the canopy interface (Figure 2.5*b*). However, unlike terrestrial systems, in aquatic systems the KH vortices are very persistent. Indeed, their strong coherence has allowed exact, positive comparison between the observed vortex frequency and that predicted from instability theory (Ghisalberti and Nepf, 2002). The persistence of KH vortices is permitted by the limited submergence depth ($H / h <\approx 5$) at which the aquatic observations have been made. The presence of the water surface constrains the maximum

scale of the boundary-layer turbulence. Because the boundary-layer and mixing-layer eddies are of similar scale, the boundary-layer eddies appear to have little impact on the coherence of the KH vortices. Indeed, the KH vortices dominate over the entire flow depth. It is likely that if the depth of submergence were to increase, that the intermittency in the KH vortices would return, even in the aquatic canopies. The numerical model described in Fitzmaurice et al., 2004, has a domain scale ten times the canopy height ($H / h = 10$), and it produced KH structures that are intermittent. Thus, it seems that the transition from persistent to intermittent structures occurs between $H / h = 5$ and 10.

The depth of submergence (H / h) also dictates the relative importance of stress-driven and potential-driven flow within the canopy, where the potential gradient includes both pressure gradient and bed slope. From a simple momentum scaling, the relative contribution of stress and potential gradients is proportional to the ratio $(H - h) / h$. For $H / h > \approx 10$ the flow within the canopy is driven only by the vertical turbulent transport of momentum from the overflow, with negligible contribution from pressure gradients. This defines the unconfined canopy regime (Figure 2.5*a*) observed

in terrestrial canopies, but also observed in some deeply submerged, sea-grass meadows. Next, for $H / h < 10$, flow is driven by both stress penetration and potential gradient (Figure 2.5*b*). Finally, in emergent canopies ($H / h = 1$, Figure 2.5*c*) the canopy flow is driven predominantly by potential gradient.

2.2.2 Flexibility

In both submerged and emergent vegetation flexible elements are distinguished from that of rigid elements because the drag coefficient of flexible vegetation decreases when the vegetation is bending (shown in Figure 2.7). In Figure 2.7, h is the erected vegetation height and h_d is the deflected plant complex than rigid vegetation. For submerged vegetation, bending of the vegetation influences the mean velocity.

For submerged flexible vegetation, three different configurations can be distinguished depending on the flow velocity and the plant characteristics. These three configurations are shown in Figure 2.7 (Dijkstra, J. T., and Uittenbogaard, R. E.,2006).

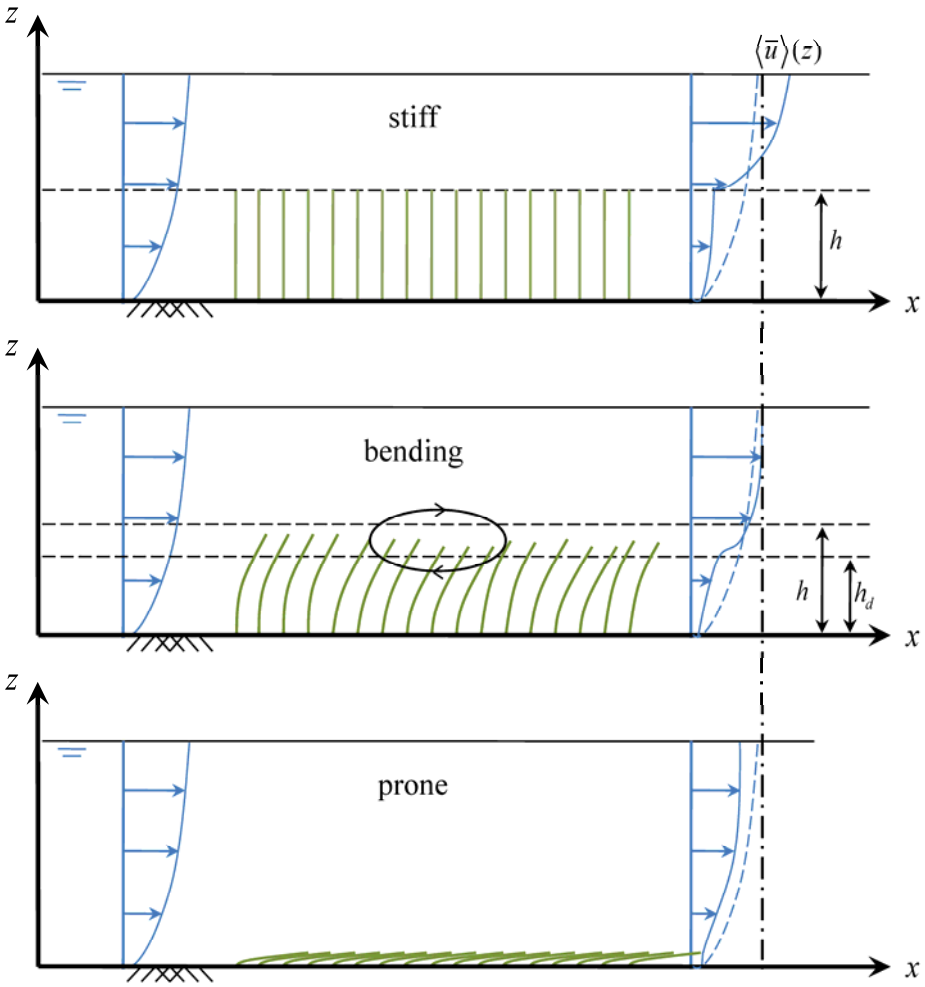

Figure 2.7 Configurations of flexible vegetation
(adapted from Dijkstra and Uittenbogaard, 2006)

1. Vegetation that is erected and do not change their position in time;

2. Vegetation that is subjected to a waving motion and, thus, change their position in time;

3. Vegetation that assumes a permanently prone position (bended forward).

At low flow velocities the flexible vegetation shows a rigid behavior. In situation 2 and 3 the behavior of the vegetation depends not only on the flow velocity but also on the bending stiffness of the vegetation. The difficulties of flexible vegetation are to determine the deflected vegetation height for each hydraulic condition and to take into account the vegetation concentration. For bending vegetation, the vegetation height changes in time leading to increases and decreases of resistance.

2.2.3 Monami of interface

Ackerman and Okubo (1993) reported the effects of a marine plant canopy on flow in the coastal environment. In addition to reducing the magnitude of the ambient flow, a Zostera marina canopy was observed to undulate under

unidirectional flow. Under some conditions, the canopy-scale vortices produce sufficient instantaneous drag to overcome the buoyancy and rigidity of individual blades. The passage of the traveling vortices then causes a local depression in the canopy, which travels along the canopy interface, in sync with the traveling vortices. This progressive waving of canopy blades is called a monami (mo = aquatic plant, nami = wave; c.f., *honami*, ho = cereal). Spectral analyses of the velocity fluctuations in the canopy revealed a fundamental frequency of approximately 0.125 ~ 0.156 Hz. These fluctuations were not caused by ambient flow conditions but rather by the hydroelasticity of the plants (monami). This monami indicates that the plants are hydroelastically translating the energy in the fluid into an approximately 6.4 ~ 6.8s cycle (Finnigan and Mulhearn 1978). Ackerman and Okubo (1993) demonstrated that flow within the canopy can be, therefore, considered a function of plant movement rather than ambient conditions and seagrass canopies provide a mechanism for particulate sedimentation through increased shear.

To date, flow through submerged aquatic vegetation has largely been viewed as perturbed boundary layer flow, with vegetative drag treated as an

extension of bed drag. However, recent studies of terrestrial canopies demonstrate that the flow structure within and just above an unconfined canopy more strongly resembles a mixing layer than a boundary layer. Specifically, all vertical profiles of mean velocity, characterized by two regions, contain an inflection point, which makes the flow susceptible to Kelvin-Helmholtz instability. This instability leads to the generation of large, coherent vortices within the mixing layer, which dominate the vertical transport of momentum through the layer. Ghisalberti and Nepf (2002) demonstrated (Figure 2.8) that the strong agreement between predicted and observed frequencies suggested that peaks in velocity spectra are associated with KH instability (Table 2.1). The downstream advection of these vortices is shown to cause the progressive, coherent waving of aquatic vegetation, known as the monami. Also Ghisalberti and Nepf (2002) found that when the monami is present, the turbulent vertical transport of momentum is enhanced, with turbulent stresses penetrating an additional 30% of the plant height into the canopy. However, if the instantaneous drag associated with the canopy-scale vortices is not sufficient to depress individual blades, the monami will not occur, even though the canopy-scale vortices are present.

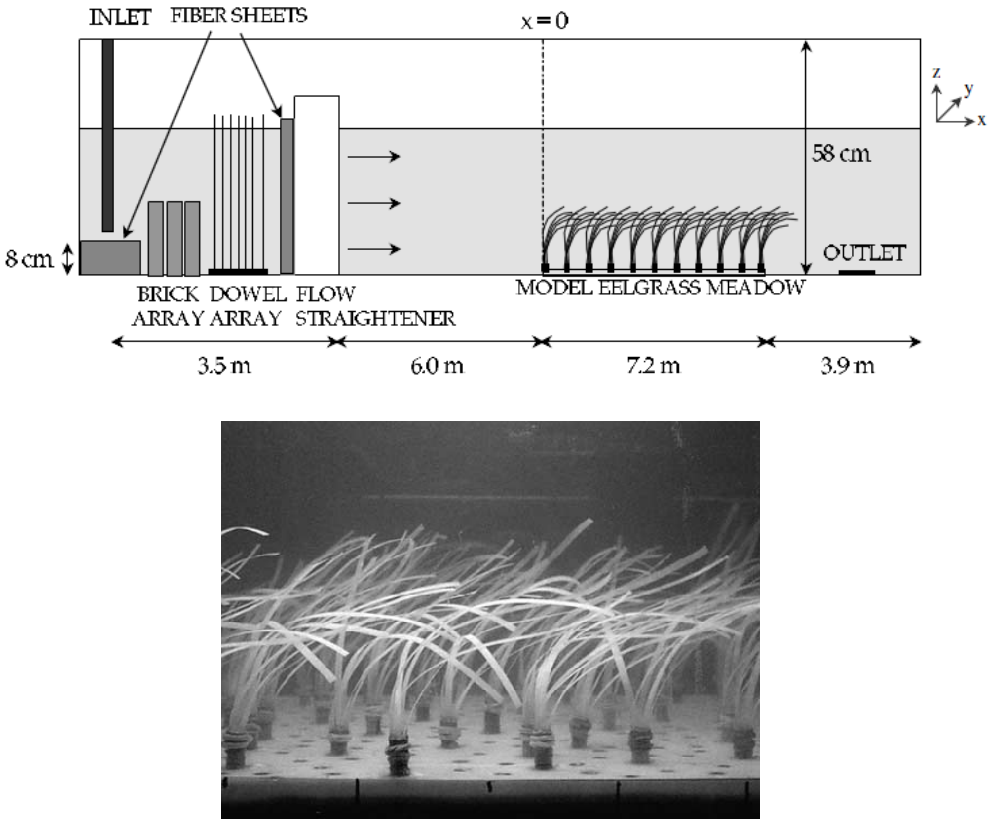

Figure 2.8 Experimental configuration in the laboratory flume and the eelgrass meadow (Ghisalberti and Nepf, 2002)

Table 2.1 Comparison of frequencies (Ghisalberti and Nepf, 2002)

Scenario	Monami frequency (Hz)	Peak frequency in spectra (Hz)	Predicted mixing layer instability frequency (Hz)
A	0.055 ± 0.008	0.052 ± 0.006	0.051 ± 0.002
B	0.028 ± 0.001	0.028 ± 0.003	0.028 ± 0.001
C	…	0.012 ± 0.001	0.010 ± 0.001
D	0.064 ± 0.003	0.063 ± 0.007	0.063 ± 0.002
E	0.039 ± 0.005	0.039 ± 0.006	0.037 ± 0.002
F	…	0.014 ± 0.002	0.012 ± 0.001
G	0.11 ± 0.01	0.11 ± 0.01	0.11 ± 0.01
H	…	0.062 ± 0.006	0.06 ± 0.003
I	…	0.11 ± 0.01	0.12 ± 0.01

3. Velocity Profile

Using flow equations for overflow region and force balance for vegetation region, a vertical two-dimensional incompressible combined flow field of waves, current, and submerged vegetation is mathematically formulated. Stream functions for these regions are separately derived using appropriate boundary conditions. Both stream functions are coupled using the interface boundary condition to derive a mathematical model for the combined wave-current vegetation flow field. Schematic diagram of wave-current flow through submerged vegetation is shown in Figure 3.1.

To formulate the wave-current flow, the two-dimensional (2D) flow through submerged vegetation is vertically divided into two regions, the lower vegetation region of stem height h_2 from the bottom where vertical coordinate $z = 0$ and the upper overflow of depth h_1 from h_2 to the free surface. Thus, $z = h_1 + h_2$ corresponds to the free surface and $z = h_2$ corresponds to an interface between vegetation and overflow. η_1 is the periodic disturbance on the free surface and η_2 is the internal wave generated at the interface due to

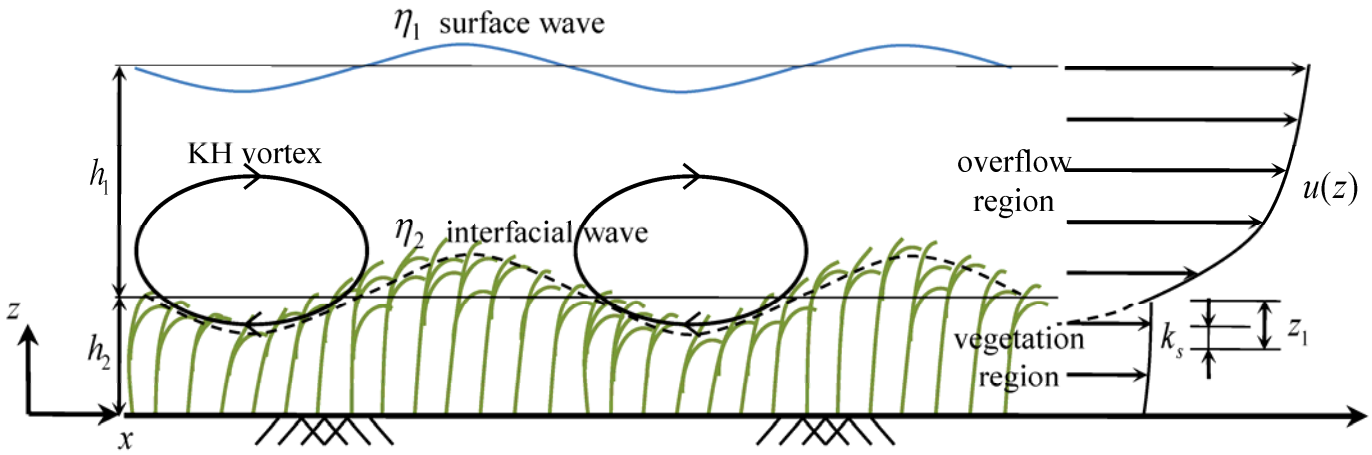

Figure 3.1 Schematic diagram of wave-current flow through submerged vegetation

interaction between two regions. For current-only flow, the current in the vegetation region is a function of vegetation drag which is constant over vegetative depth and the flow is a balance of pressure gradient and vegetative drag. Therefore, the vertical profile of longitudinal velocity remains constant over depth in the vegetated region, whereas it is logarithmic in the overflow region. Ghisalberti and Nepf (2005) said that in the presence of wave activity, the wave motion enhances the convective velocity in overflow region owing to the drift velocity, whereas in the vegetative region it enhances turbulence. Hence, the flow is essentially described by two separate stream functions, ψ_1 and ψ_2 for the overflow and the vegetation region, respectively; each comprises current and wave components. The logarithmic profile in the overflow region is available on a virtual bed (z_1) little below the top of the vegetation (Nepf and Vivoni 2000). The flow within the depth $h_1 + z_1$ is governed by ψ_1, whereas below this level until the channel bottom it is governed by ψ_2. The exact point of change over from ψ_1 to ψ_2 is calculated in the following formulation by simultaneously solving for overflow and vegetation velocity profiles.

3.1 Overflow region

The vertical range of the overflow region (Figure 3.2) is $\left[(h_2 - z_1 + k_s) < z < (h_1 + h_2 + \eta_1)\right]$. In this section, a combined stream function for the wave-log current is derived. The resultant formulation is in the form of a combined stream function $\psi_1(x,z,t)$ for 2D incompressible steady flow with a surface periodic wave, where x is the flow direction, z is the vertical direction from the channel bottom, and t is the time. Thus, the log current for turbulent flow velocity u_1 can be written as

$$u_1 = \frac{u_*}{\kappa}\log\frac{z_0}{z_s} + U_c \qquad (3.1a)$$

for

$$z_0 = z - (h_2 - z_1 + k_s);\ z_0 \geq 0 \ \text{ and } \ z_s = (h_2 - z_1) + k_s \qquad (3.1b)$$

where $U_c = 3.7u_*$ (Nezu and Nakagawa 1993); $u_* = \sqrt{gh_oS_b}$ = shear velocity; $h_o = h_1 + z_1 - k_s$; S_b = surface energy gradient; k_s = Nikuradse's bottom roughness height; and $\kappa = 0.4$ = von Karman constant. Nezu and Nakagawa (1993) stated that Eq. (3.1a) is valid near the bottom region. However, in practical applications Eq. (3.1a) is still commonly assumed to describe the

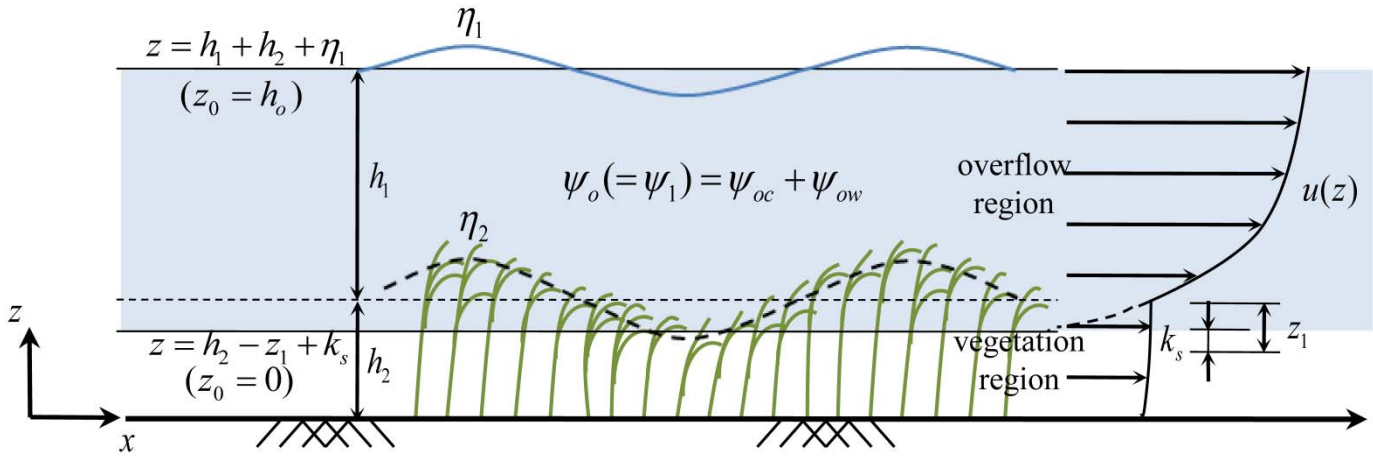

Figure 3.2 Overflow region

velocity distribution over the entire depth of uniform steady open-channel flows. The quantity z_o is the new origin after vertically shifting from its original location of channel bottom. This shift of origin is because the logarithmic velocity profile is applicable only from vertical exchange zone ($z_1 - k_s$) to overflow region (Nepf and Vivoni 2000). The logarithmic profile becomes asymptotic with the x axis at z_1 distance below the interface. This location from the channel bottom is equal to $h_2 - z_1$. Thus, Eq. (3.1*a*) is applicable for $z_0 \geq 0$. Moreover, Prandtl's hypothesis suggests that the velocity crosses the z axis a little above the distance $h_2 - z_1$ called the virtual bed. This distance is Nikuradse's roughness height (k_s) (Polatel, 2006). Thus, from the channel bottom the location of the lower end (crossing point with the z axis) of the depthwise log current is equal to $h_2 - z_1 + k_s$. To derive the combined stream function,

$$\psi_c = \int u_1 dz_0 = \frac{u_*}{\kappa}\left(z_0 \log\frac{z_0}{z_s} - z_0 \right) + U_c z_0 + B_1 \qquad (3.2)$$

is considered (B_1 is a constant and is zero for the horizontal bottom) and the stream function for the wave component influenced by the current part will be derived using the wave theory. The approach is given by Baddour and Song

(1998), who assumed wave component a priori and derived the current component which is a depthwise linear current profile.

3.1.1 Governing equations

To derive the combined stream function for wave-log current, the equations of motion with the viscous effect neglected, and the gravitational body force included, can be written as

$$\rho\left(\frac{\partial u}{\partial t}+u\frac{\partial u}{\partial x}+w\frac{\partial u}{\partial z_0}\right)=-\frac{\partial p}{\partial x} \tag{3.3a}$$

$$\rho\left(\frac{\partial w}{\partial t}+u\frac{\partial w}{\partial x}+w\frac{\partial w}{\partial z_0}\right)=-\frac{\partial p}{\partial z_0}-\rho g \tag{3.3b}$$

where $\rho =$ constant water density; p = pressure in the overflowing fluid; and g = acceleration due to gravity. Also $u=\partial\psi_1/\partial z_0$ and $w=-\partial\psi_1/\partial x$ are the velocity components in the x and z_o directions, respectively, where ψ_1 is the stream function for the overflow region. Eqs. (3.3*a*) and (3.3*b*) are integrated over x and z_o, respectively. Using the continuity equation $\partial u/\partial x+\partial w/\partial z_0=0$ and conservation of vorticity and eliminating pressure terms, the resultant 2D equation of motion is written as

$$\frac{\partial^2 u}{\partial t \partial z_0} + u\frac{\partial^2 u}{\partial x \partial z_0} + w\frac{\partial^2 u}{\partial^2 z_0} + \frac{\partial u}{\partial z_0}\left(\frac{\partial u}{\partial x} + \frac{\partial w}{\partial z_0}\right)$$
$$= \frac{\partial^2 w}{\partial t \partial x} + u\frac{\partial^2 w}{\partial^2 x} + w\frac{\partial^2 w}{\partial z_0 \partial x} + \frac{\partial w}{\partial x}\left(\frac{\partial u}{\partial x} + \frac{\partial w}{\partial z_0}\right) \tag{3.4a}$$

$$\left(\frac{\partial}{\partial t} + \mathbf{V}\cdot\nabla\right)\nabla^2\psi = 0 \tag{3.4b}$$

where ∇ is the two-dimensional differential operator $\mathbf{i}(\partial/\partial x) + \mathbf{j}(\partial/\partial y)$, ∇^2 is the two-dimensional Laplacian operator $(\partial^2/\partial x^2 + \partial^2/\partial y^2)$, and $\mathbf{V} = \partial\psi_1/\partial z_0\mathbf{i} - \partial\psi_1/\partial x\mathbf{j}$ = velocity vector. Substitution of $\mathbf{V}$ in Eq. (3.4*b*) yields

$$\left[\frac{\partial^3\psi_1}{\partial t\partial x^2} + \frac{\partial^3\psi_1}{\partial t\partial z_0^2}\right] + \frac{\partial\psi_1}{\partial z_0}\left[\frac{\partial^3\psi_1}{\partial x^3} + \frac{\partial^3\psi_1}{\partial x\partial z_0^2}\right] - \frac{\partial\psi_1}{\partial x}\left[\frac{\partial^3\psi_1}{\partial z_0\partial x^2} + \frac{\partial^3\psi_1}{\partial z_0^3}\right] = 0 \tag{3.4c}$$

The coordinate axis (x, z_o) is fixed at the virtual bottom, where $z_o = \eta(x,t)$ on the free surface, which is assumed to be a periodic function.

3.1.2 Boundary conditions

As the flow below the virtual bottom is depthwise constant and unidirectional through vegetation, the only flux across the bottom of overflow will be the periodic flux owing to the existence of interfacial internal wave. Accordingly,

the bottom boundary condition is written as

$$\frac{\partial \psi_1}{\partial x} = -w_1\big|_{z_0=0} \tag{3.5}$$

whereas on the free surface, the pressure is zero. In Eq. (3.5), w_1 = vertical velocity at $z_o = 0$. The free-surface kinematic boundary condition is

$$\left(\frac{\partial}{\partial t} + \mathbf{V}\cdot\nabla\right) S = 0 \quad \text{on} \quad z_0 = \eta_1(x,t) \tag{3.6}$$

and the periodic and permanent type free surface is given by

$$S(x, z_0, t) = z_0 - \eta_1(x,t) = 0 \tag{3.7}$$

where

$$\eta_1(x,t) = h_1 + h_2 + \sum_{n=1}^{\infty} a_n \cos n(kx - \sigma t) \tag{3.8}$$

is the elevation of free surface from the channel bottom expressed in a Fourier series in ($kx - \sigma t$), a_n = Fourier coefficients; $k = 2\pi / L$ = wave number; and $\sigma = 2\pi / T$ = wave frequency, where L and T are the wavelength and wave period, respectively. The dynamic boundary conditions to the first order in terms of the stream function is given by

$$-g\frac{\partial \eta_1}{\partial x} + \frac{\partial}{\partial x}\int\left[\frac{\partial^2 \psi_1}{\partial t \partial x} + \frac{\partial \psi_1}{\partial z_0}\frac{\partial^2 \psi_1}{\partial x^2} - \frac{\partial \psi_1}{\partial x}\frac{\partial^2 \psi_1}{\partial x \partial z_0}\right] dz_0 = 0 \qquad \text{at} \quad z_0 = h_1 + z_1 - k_s \tag{3.9}$$

which is used for the celerity for the overflow region.

3.1.3 Stream function of overflow region

To find the stream function ψ_1 of overflow region, Eq. (3.4*c*) is solved with the boundary conditions given by Eqs. (3.5), (3.6), and (3.9). The assumption introduced to solve this boundary value problem is that the free surface motion is periodic and of permanent type. η_1 must be a periodic function. From the periodicity of η_1, it follows that ψ_1 must also be a periodic function such that $\psi_1(x, z_0, t) = \psi_1(kx - \sigma t, z_0)$ for the horizontal bed and can be written as

$$\psi_1(x, z_0, t) = \sum_{n=0}^{\infty} A_n(z_0) \cos n(kx - \sigma t) \tag{3.10}$$

where $A_n(z_o)$ = Fourier coefficients of z_0 only and to be determined. To determine the functions $A_n(z_o)$, the solution of Eq. (3.4*c*) has to be found satisfying the boundary conditions of Eqs. (3.5), (3.6), and (3.9). The strategy of finding these functions is firstly to decide the order of the solution. Secondly, to find $A_n(z_o)$, $\psi_1(x, z_0, t)$ satisfies the fundamental governing Eq. (3.4*c*) and the bottom boundary condition (Eq. (3.5)). Thirdly, the kinematic

and dynamic free surface conditions (Eqs. (3.6) and (3.9)) are used to determine the coefficients a_n, in Eq. (3.7), and the dispersion relation of the free surface motion. These steps are presented in detail in the following section.

3.1.4 The first order solution

Eqs. (3.7) and (3.10) which are the expressions for η_1 and ψ_1 to the first-order expansion can be written as

$$\eta_1(x,t) = h_1 + h_2 + a\cos(kx - \sigma t) \tag{3.11}$$

and

$$\psi_1(x, z_0, t) = A_0(z_0) + A_1(z_0)\cos(kx - \sigma t) \tag{3.12}$$

where a = surface wave amplitude. First of all, to derive the expressions for A_0 and A_1, the boundary value problem formed by the Eq. (3.4*c*), and the boundary conditions should be satisfied to the first order in the wave amplitude a. The stream function $A_0(z_0) = \psi_c$ is given by Eq. (3.2). The expression for A_1 in Eq. (3.12) is obtained by substituting Eq. (3.2) in Eq. (3.12) and then Eq. (3.12) in Eq. (3.4*c*) as

$$\left\{\sigma A_1'' - \sigma k^2 A_1 + U_c k^3 A_1 + \left(\frac{u_*}{\kappa} k^3 \log\frac{z_0}{z_s}\right) A_1 - U_c k A_1'' - \left(\frac{u_*}{\kappa} k \log\frac{z_0}{z_s}\right) A_1'' \right.$$
$$\left. - \frac{u_* k}{\kappa z_0^2} A_1 \right\} \sin(kx - \sigma t) + \left\{-k A_1' A_1'' + k A_1' A_1'''\right\} \frac{\sin 2(kx - \sigma t)}{2} = 0 \tag{3.13}$$

where the prime denotes differentiation with respect to z_o. Eq. (3.13) suggests that for all $(kx - \sigma t)$, a set of ordinary differential equations are

$$\sigma A_1'' - \sigma k^2 A_1 + U_c k^3 A_1 + \left(\frac{u_*}{\kappa} k^3 \log\frac{z_0}{z_s}\right) A_1 - U_c k A_1''$$
$$- \left(\frac{u_*}{\kappa} k \log\frac{z_0}{z_s}\right) A_1'' - \frac{u_* k}{\kappa z_0^2} A_1 = 0 \tag{3.14}$$

and

$$-k A_1' A_1'' + k A_1' A_1''' = 0 \tag{3.15}$$

A prime denotes differentiation with respect to z_o. Eq. (3.15) is the differential equation for wave-only flow for which the solution satisfying Eq. (3.5) is

$$A_1(z_0) = \beta_1 \sinh(m z_o) = \beta_1 \sinh(k z_o) \tag{3.16}$$

where β_1 = constan to be determined and $m = k$. For $m > k$ and $m < k$, trigonometric current profiles are outside of the scope of the present investigation. That's because when $m = k$, it is clear that the solution represents a periodic wave that propagates with permanent form on a linearly

distributed current. Moreover, when $\beta_1 = 0$, the function ψ_1 reduces to the solution of the potential problem, which describes waves on a uniform current (Baddour and Song, 1998). Substitution of Eq. (3.16) in Eq. (3.14) results in $-(u_* k / \kappa z_0^2)\beta_1 \sinh(kz_0) = 0$. This expression satisfies the condition of $\sinh\left[k(h_1 + z_1 - k_s)\right] \to 0$, which is true for shallow water waves $\left\{(h_1 + z_1 - k_s) / L < 0.05\right\}$. Thus, Eq. (3.14) satisfies Eq. (3.2) and therefore validates the assumed log-current profile. Substituting A_0 and A_1 in Eq. (3.12), the stream function for the combined wave-current rotational flow field is

$$\psi_1(x, z_0, t) = \frac{u_*}{\kappa}\left(z_0 \log\frac{z_0}{z_s} - z_0 \right) + U_c z_0 + \beta_1 \sinh(kz_o)\cos(kx - \sigma t) \qquad (3.17a)$$

where the first two terms on the right side are the steady current components the second term $U_c z_o$ represents the depthwise constant velocity; as eliminated henceforth, and the third term is the first-order wave motion. Thus Eq. (3.17*a*) can be written in a more concise form as

$$\psi_1(x, z_0, t) = \frac{u_*}{\kappa}\left(z_0 \log\frac{z_0}{z_s} - z_0 \right) + \beta_1 \sinh(kz_o)\cos(kx - \sigma t) \qquad (3.17b)$$

The resulting first term properly represents the log-current profile. Coefficient β_1 in Eq. (3.17*b*) now can be determined by Taylor's expansion of the

kinematic free surface boundary condition about $z_0 = h_1 + z_1 - k_s$ to the first order, i.e., using Eq. (3.6). Thus, Eq. (3.7) and as $\partial z_0 / \partial t = 0$, $\partial z_0 / \partial x = 0$ and $\partial \eta_1 / \partial z_0 = 0$; expanding Eq. (3.6) yields the kinematic surface condition:

$$\frac{\partial \eta_1}{\partial t} + \frac{\partial \psi_1}{\partial z_0}\frac{\partial \eta_1}{\partial x} + \frac{\partial \psi_1}{\partial x} = 0 \tag{3.18}$$

Substituting Eqs. (3.11) and (3.17*b*) in Eq. (3.18) one gets

$$\begin{aligned} &a\sigma \sin(kx - \sigma t) - \frac{u_*}{\kappa} ak \log\frac{30 z_0}{z_s}\sin(kx - \sigma t) \\ &-\frac{ak^2}{2}\beta_1 \sin 2(kx - \sigma t)\cosh(kz_o) - \beta_1 k \sinh(kz_o)\sin(kx - \sigma t) = 0 \end{aligned} \tag{3.19}$$

The term consisting of $\sin 2(kx - \sigma t)$ corresponds to the second order expansion and is hence neglected. From the remaining terms and applying at $z_0 = h_1 + z_1 - k_s$, β_1 can be given as

$$\beta_1 = \frac{a\left[c - \frac{u_*}{\kappa}\log\frac{\left(h_1 + z_1 - k_s\right)}{z_s}\right]}{\sinh\left[k\left(h_1 + z_1 - k_s\right)\right]} \tag{3.20}$$

and $c = \sigma / k$ is determined. Substituting Eq. (3.19) in Eq. (3.17*b*), the stream function for the overflow region is expressed as

$$\begin{aligned} \psi_1(x, z_0, t) = &\frac{u_*}{\kappa}\left(z_0 \log\frac{z_0}{z_s} - z_0\right) \\ &+ \frac{a\left[c - \frac{u_*}{\kappa}\log\frac{\left(h_1 + z_1 - k_s\right)}{z_s}\right]}{\sinh\left[k\left(h_1 + z_1 - k_s\right)\right]}\sinh(kz_o)\cos(kx - \sigma t) \end{aligned} \tag{3.21}$$

The dynamic free surface condition is now used to determine the dispersion relation. The pressure *p* is assumed to be constant such that:

$$\frac{\partial p}{\partial x} = 0 \qquad \text{on} \quad z_0 = \eta_1(x,t) \tag{3.22}$$

Substituting Eqs. (3.11) and (3.21) in the dynamic boundary condition (Eq. (3.9)) and applying at $z_0 = h_1 + z_1 - k_s$ on gets

$$\begin{aligned}
&-gka + k\sigma \frac{a\left[c - \frac{u_*}{\kappa}\log\frac{(h_1 + z_1 - k_s)}{z_s}\right]}{\sinh\left[k(h_1 + z_1 - k_s)\right]}\cosh\left[k(h_1 + z_1 - k_s)\right] \\
&-k^2 \frac{a\left[c - \frac{u_*}{\kappa}\log\frac{(h_1 + z_1 - k_s)}{z_s}\right]}{\sinh\left[k(h_1 + z_1 - k_s)\right]} T_1\left(\frac{u_*}{\kappa}\right) \\
&+k^2 \frac{a\left[c - \frac{u_*}{\kappa}\log\frac{(h_1 + z_1 - k_s)}{z_s}\right]}{\sinh\left[k(h_1 + z_1 - k_s)\right]}\left(\frac{u_*}{\kappa}\right)\log\left(\frac{h_1 + z_1 - k_s}{z_s}\right)\cosh\left[k(h_1 + z_1 - k_s)\right] = 0
\end{aligned} \tag{3.23}$$

where $T_1 = \log[(h_1 + z_1 - k_s)/z_s] + [k(h_1 + z_1 - k_s)]^2/4$. Applying the shallow water approximation, i.e., $\cosh[k(h_1 + z_1 - k_s)] \approx 1$, $\sinh[k(h_1 + z_1 - k_s)]$ $\approx k(h_1 + z_1 - k_s)$, the above equation with $h_o = h_1 + z_1 - k_s$ becomes

$$\begin{aligned}
&gka(kh_o) - ka\sigma\left[c - \frac{u_*}{\kappa}\log\frac{h_o}{z_s}\right] + k^2 a\left[c - \frac{u_*}{\kappa}\log\frac{h_o}{z_s}\right]\left(\frac{u_*}{\kappa}\right)\log\frac{h_o}{z_s} \\
&-k^2 a\left[c - \frac{u_*}{\kappa}\log\frac{h_o}{z_s}\right]\left(\frac{u_*}{\kappa}\right)\left\{\log\frac{h_o}{z_s} + \frac{(kh_o)^2}{4}\right\} = 0
\end{aligned} \tag{3.24}$$

The celerity of overflow can be written as

$$c = \frac{u_*}{\kappa}\left[\log\frac{h_o}{z_s} - \frac{1}{2}\left\{\log\frac{h_o}{z_s} + \frac{(kh_o)^2}{4}\right\}\right] \pm \frac{1}{2}\sqrt{\left(\frac{u_*}{\kappa}\right)^2\left\{\log\frac{h_o}{z_s} + \frac{(kh_o)^2}{4}\right\}^2 + 4gh_o} \tag{3.25}$$

The corresponding dispersion equation explicit in σ for the overflow region is

$$\sigma = \frac{u_* k}{\kappa}\left[\log\frac{h_o}{z_s} - \frac{1}{2}\left\{\log\frac{h_o}{z_s} + \frac{(kh_o)^2}{4}\right\}\right] \pm \frac{1}{2}\sqrt{\left(\frac{u_* k}{\kappa}\right)^2\left\{\log\frac{h_o}{z_s} + \frac{(kh_o)^2}{4}\right\}^2 + 4k^2 gh_o} \tag{3.26}$$

If $u_* = 0$ (i.e., shear current is removed), Eq. (3.26) reduces to the dispersion equation for wave-only case (Dean and Dalrymple, 1991); $\sigma^2 = gk\tanh(kh_o)$ and with $\tanh(kh_o) \approx kh_o$, it is

$$\sigma = k\sqrt{gh_o} \tag{3.27}$$

To derive the dispersion coefficient for the vortex-overflow, the combined horizontal velocity can be derived as

$$U = \frac{\partial \psi_1}{\partial z_0} = \frac{u_*}{\kappa}\log\frac{z_0}{z_s} + k\frac{a\left[c - \frac{u_*}{\kappa}\log\frac{(h_1 + z_1 - k_s)}{z_s}\right]}{\sinh\left[k(h_1 + z_1 - k_s)\right]}\cosh(kz_o)\cos(kx - \sigma t) \tag{3.28}$$

where β_1 is as given by Eq. (3.20) (Figures 3.3 and 3.4). Averaging Eq. (3.28) over h_o, which is $h_1 + z_1 - k_s$, the depth-averaged velocity is

$$\bar{U} = \frac{u_*}{h_o}\left\{\frac{h_o}{\kappa}\log\frac{h_o}{z_s} - h_o\beta_1\cos(kx-\sigma t)\sinh(kh_o)\right\}$$
$$= \frac{u_*}{\kappa}\log\frac{h_o}{z_s} - u_*\beta_1\cos(kx-\sigma t)\sinh(kh_o) \quad (3.29)$$

Because the LDC of overflow region significantly affects the total LDC of whole water body comparing to that of vegetation one, characteristics determining the LDC has to be checked with respect to submergence depth. Vector diagrams of longitudinal ($\partial\psi_1/\partial z_0$) and vertical velocity ($\partial\psi_1/\partial x$) depending on $H/h = 3$ and $H/h = 12$ shows the effect of vortices. In Figure 3.3, vortex is allowed to penetrate deeper than relatively large submergence depth (Figure 3.4), which corresponds with previous experimental research of Ghisalberti and Nepf (2002).

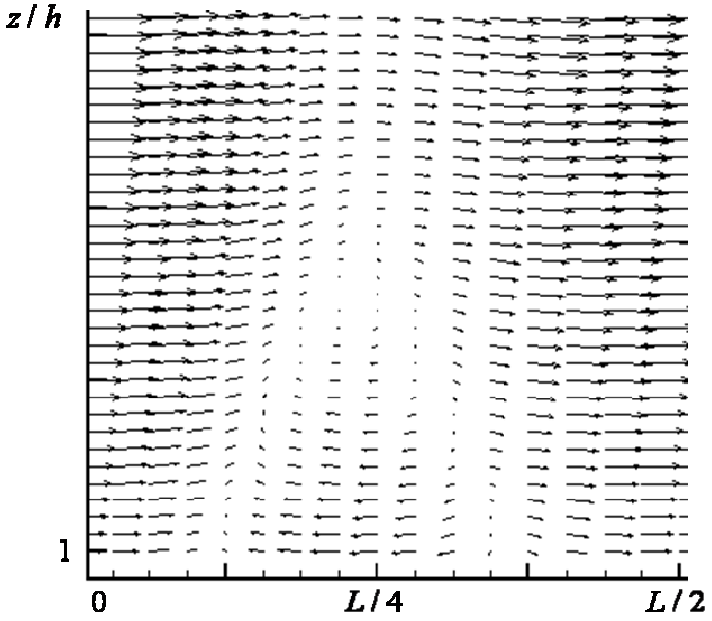

Figure 3.3 Vector diagrams of submergence depth, $H / h = 3$

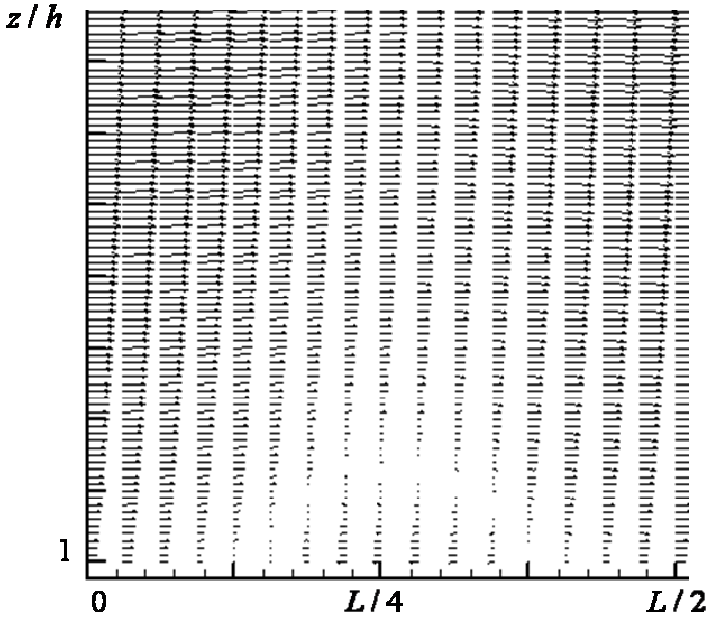

Figure 3.4 Vector diagrams of submergence depth , $H / h = 12$

3.2 Vegetation region

For flow in the vegetation region $\left[0 < z < \left(h_2 - z_1 + k_s\right)\right]$ (as shown in Figure 3.5), there is a balance between the drag force and the pressure gradient which can be written as

$$\frac{1}{2}\rho C_D d N u_2^2 = g\rho i \tag{3.30}$$

where ρ = constant density; i = energy gradient; C_D = drag coefficient; d = stem diameter; g = acceleration due to gravity; N = number of stems per unit area; and u_2 = depthwise constant flow velocity in the vegetation region. Strictly speaking, in the longitudinal exchange zone ($h_2 - z_1 + k_s$) (Nepf and Vivoni, 2000), u_2 can be given from Eq. (3.30) as

$$u_2 = \sqrt{\frac{2gi}{C_D dN}} \tag{3.31}$$

To include the periodicity induced from surface waves in the overflow region, first $u_2 = \partial\psi_2 / \partial z$ is substituted in Eq. (3.30)

$$\frac{1}{2}\rho C_D dN\left(\frac{\partial\psi_2}{\partial z}\right)^2 = g\rho i \tag{3.32}$$

and a combined wave-current stream function to the first order for the vegetation region is assumed in the following form:

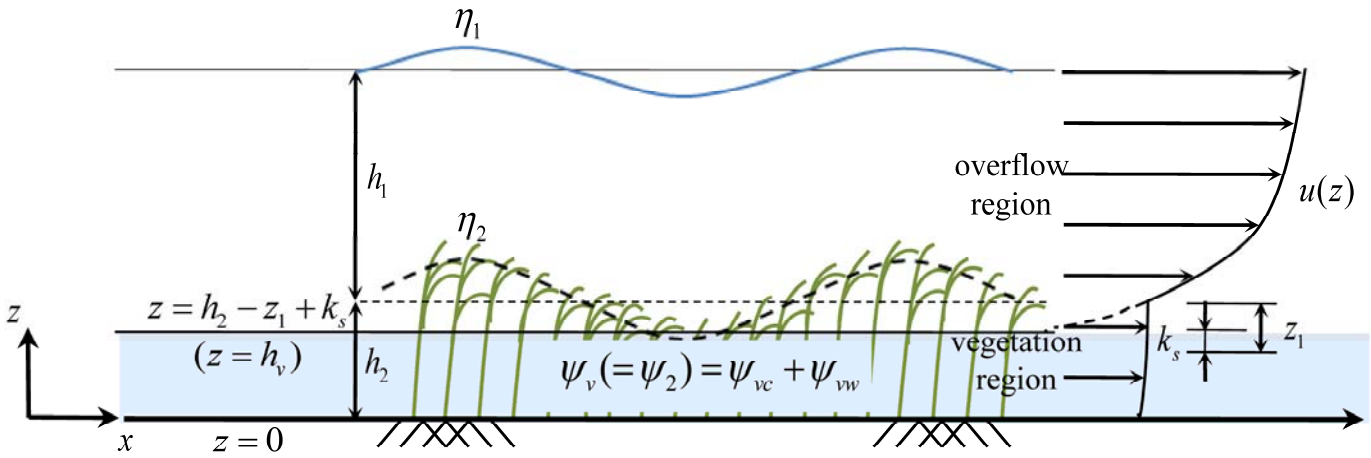

Figure 3.5 Vegetation region

$$\psi_2(x,z,t) = A_{0v}(z) + A_{1v}(z)\cos(kx - \sigma t) \tag{3.33}$$

where the current-only part $A_{0v} = u_2 z + B_2 = \sqrt{(2gi / C_D dN)}z + B_2$ can be obtained by integrating Eq. (3.30) over depth. Furthermore, $B_2 = 0$ can be set by using flat bottom boundary condition for which A_{0v}, $A_{1v} = 0$ at $z = 0$. Substituting A_{0v} in Eq. (3.33), Eq. (3.33) can be written as

$$\psi_2(x,z,t) = u_2 z + A_{1v}(z)\cos(kx - \sigma t) \tag{3.34}$$

Eq. (3.34) is substituted in Eq. (3.4*c*) to get

$$\begin{aligned}&\left\{\sigma A_{1v}'' - \sigma k^2 A_{1v} + u_2 k^3 A_{1v} - u_2 k A_{1v}''\right\}\sin(kx - \sigma t)\\ &+\left\{k^3 A_{1v} A_{1v}' - k A_{1v}' A_{1v}'' - k^3 A_{1v} A_{1v}' + k A_{1v} A_{1v}'''\right\}\frac{\sin 2(kx - \sigma t)}{2} = 0\end{aligned} \tag{3.35}$$

where the prime denotes differentiation with respect to *z*. For all $(kx - \sigma t)$, the above equation simplifies to a set of differential equations as

$$\sigma A_{1v}'' - \sigma k^2 A_{1v} + u_2 k^3 A_{1v} - u_2 k A_{1v}'' = 0 \tag{3.36a}$$

and

$$-k A_{1v}' A_{1v}'' + k A_{1v} A_{1v}''' = 0 \tag{3.36b}$$

The solution of Eq. (3.36*b*) with no-flux bottom boundary condition mentioned above provides

$$A_{1v}(z) = \beta_2 \sinh(kz) \tag{3.37}$$

Eq. (3.37) in turn satisfies Eq. (3.36*a*) and hence satisfies Eq. (3.4*c*). Eq. (3.33) becomes

$$\psi_2(x,z,t) = A_{0v}(z) + \beta_2 \sinh(kz)\cos(kx - \sigma t) \tag{3.38}$$

This stream function is applicable from the channel bottom ($z = 0$) up to the point where it touches the logarithmic profile of overflow. If this point is at a distance of, say, k_s above z_1 then its position from the channel bottom is $z = h_2 - z_1 + k_s$. The magnitude of k_s can be calculated by equating both the overflow and vegetation profiles (i.e., Eqs. (3.1*a*) and (3.31)) and solving simultaneously, as follows:

$$\frac{u_*}{\kappa}\log\frac{30\left[z-(h_2-z_1+k_s)\right]}{(h_2-z_1)+k_s} = \sqrt{\frac{2gi}{C_D dN}} \tag{3.39}$$

and on simplifying, it is

$$z = (h_2 - z_1 + k_s) + \frac{(h_2 - z_1) + k_s}{30} e^{\frac{\kappa}{u_*}\sqrt{\frac{2gi}{C_D dN}}} \tag{3.40}$$

Eq. (3.40) provides the distance of point k_s from the channel bottom. From z_o, the distance of the same point is equal to $[(h_2 - z_1 + k_s)/30]e^{(\kappa/u_*)\sqrt{(2gi/C_D dN)}}$. To find the expression for interfacial internal wave, the interfacial condition can be stated as

$$w_1 = -\frac{\partial \psi_1}{\partial x} = \frac{\partial \eta_2}{\partial t} = w_2 \quad \text{at } z = h_2 \tag{3.41}$$

where w_1 and w_2 = vertical velocities in overflow and vegetated regions, respectively, and η_2 = interfacial wave surface applicable at $z_o = z_1 - k_s$ (replacing $z = h_2$ in Eq. (3.1*b*) provides $z_o = z_1 - k_s$). Substituting Eq. (3.17*b*) in Eq. (3.41) one finds η_2 as

$$\eta_2 = \frac{k\beta_1 \sinh\left[k(z_1 - k_s)\right]}{\sigma}\cos(kx - \sigma t) \tag{3.42}$$

where β_1 is given by Eq. (3.20). Eq. (3.42) suggests that the internal wave is in phase with the surface wave given by Eq. (3.11). Furthermore, to find β_2, Eqs. (3.38) and (3.42) are substituted in the kinematic boundary condition Eq. (3.18) as

$$\left\{k\beta_1 \sinh\left[k(z_1 - k_s)\right] - \frac{u_2 k^2 \beta_1}{\sigma}\sinh\left[k(z_1 - k_s)\right] - \beta_2 k \sinh(kz)\right\}\sin(kx - \sigma t)$$
$$-\left\{\frac{k^2 \beta_1 \beta_2}{2\sigma}\cosh(kz)\sinh\left[k(z_1 - k_s)\right]\right\}\sin 2(kx - \sigma t) = 0 \tag{3.43}$$

Eliminating the higher order term with $\sin 2(kx - \sigma t)$; for all $(kx - \sigma t)$, the remaining terms applied at $z = h_2 - z_1 + k_s$ provide an expression for β_2 as

$$\beta_2 = \frac{\beta_1\left[1 - \frac{u_2}{c}\right]\sinh\left[k(z_1 - k_s)\right]}{\sinh\left[k\left(h_2 - z_1 + k_s\right)\right]} \tag{3.44}$$

The stream function for the vegetated region can be written as

$$\psi_2(x,z,t)$$
$$= u_2 z + \frac{a\left[c - \frac{u_*}{\kappa}\log\frac{(h_1 + z_1 - k_s)}{z_s}\right]\left[1 - \frac{u_2}{c}\right]\sinh\left[k(z_1 - k_s)\right]}{\sinh\left[k\left(h_1 + z_1 - k_s\right)\right]\sinh\left[k\left(h_2 - z_1 + k_s\right)\right]}\sinh(kz)\cos(kx - \sigma t) \tag{3.45}$$

The range of Eq. (3.45) is $0 \le z \le h_2 - z_1 + k_s$, whereas for Eq. (3.21), it is $h_2 - z_1 + k_s \le h_1 + h_2$. To obtain the celerity in the vegetation region, Eqs. (3.42) and (3.45) are substituted in Eq. (3.9). This condition is as follows:

$$-g\frac{\partial \eta_2}{\partial x} + \frac{\partial}{\partial x}\int\left[\frac{\partial^2 \psi_2}{\partial t \partial x} + \frac{\partial \psi_2}{\partial z}\frac{\partial^2 \psi_2}{\partial x^2} - \frac{\partial \psi_2}{\partial x}\frac{\partial^2 \psi_2}{\partial x \partial z}\right]dz$$
$$= g\frac{k^2\beta_1}{\sigma}\sinh\left[k(z_1 - k_s)\right]\sin(kx - \sigma t) - k^3\sigma\beta_1\cosh(kz)\sin(kx - \sigma t)$$
$$+ u_2 k^2 \beta_2 \cosh(kz)\sin(kx - \sigma t) = 0 \tag{3.46}$$

and it provides the celerity as

$$c = \frac{\frac{u_2\beta_2}{k} \pm \sqrt{\left(\frac{u_2\beta_2}{k}\right)^2 + 4g\beta_1^2(z_1 - k_s)}}{2k\beta_1} \tag{3.47}$$

Eq. (3.47) is applied for shallow wave conditions, as described for overflow. The corresponding dispersion relation explicit in σ can be obtained from Eq. (3.47) as

$$\sigma = \frac{\frac{u_2\beta_2}{k} \pm \sqrt{\left(\frac{u_2\beta_2}{k}\right)^2 + 4g\beta_1^2(z_1 - k_s)}}{2\beta_1} \tag{3.48}$$

It can be seen that Eq. (3.48) with $u_2 = 0$ reduces to Eq. (3.27) for wave-only case.

To derive the dispersion coefficient for the vortex-overflow, the combined horizontal velocity can be derived as

$$U = \frac{\partial \psi_2}{\partial z} = u_2 + k\beta_2 \cosh(kz)\cos(kx - \sigma t) \tag{3.49}$$

Averaging Eq. (3.49) over h_v, which is $h_2 - z_1 + k_s$, the depth-averaged velocity is

$$\bar{U} = \frac{1}{h_v}\left\{u_2 h_v + \beta_2 \sinh(kh_v)\cos(kx - \sigma t)\right\} \tag{3.50}$$

4. Longitudinal Dispersion Coefficient

4.1 Modified Two-box model

Previously yielded final solution of Two-box model (Eq. (2.11)) is modified and Table 4.1 shows the differences between two models. Hence, the equation of the longitudinal dispersion coefficient for submerged flexible vegetation is

$$K_{\mathrm{sf}} = \frac{\left(\frac{h_o}{H}\right)^2 \left(\frac{h_v}{H}\right)^2 (U_o - U_v)^2}{b} + \left(\frac{h_o}{H}\right) K_o + \left(\frac{h_v}{H}\right) K_v . \tag{4.1}$$

and thus, the exchange coefficient, b , is

$$b^{-1} \simeq \frac{h_v^2}{D_w} + \frac{h_o}{k} + \frac{h_o^2}{\left[\frac{1}{h_o}\int_{h_v}^{H} D_z dz\right]} \tag{4.2}$$

4.1.1 Vortex-driven exchange

In sparse canopies $z_1 / h_v << 1$ and exchange is driven by the KH vortices that penetrate deep into the canopy. Experiments by Ghisalberti and Nepf (2005)

Table 4.1 Differences between two models

	Murphy et al. (2007)	This study
Schematic diagram	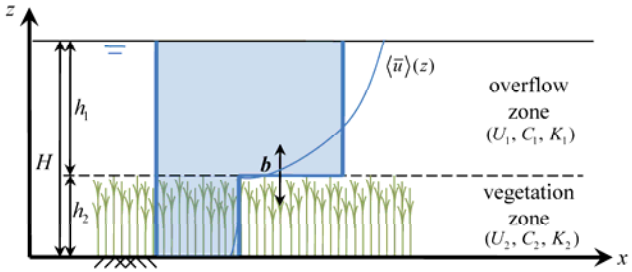	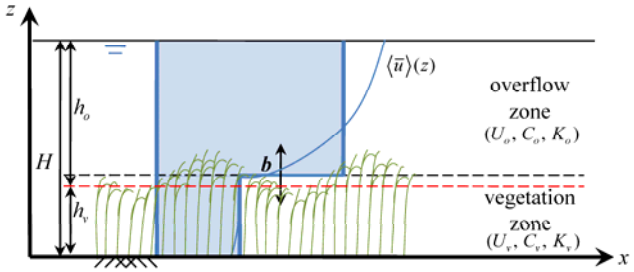
LDC	$K_{ss} = \frac{\left(\frac{h_1}{H}\right)^2\left(\frac{h_2}{H}\right)^2 (U_2 - U_1)^2}{b} + \left(\frac{h_1}{H}\right)K_1 + \left(\frac{h_2}{H}\right)K_2$	$K_{sf} = \frac{\left(\frac{h_o}{H}\right)^2\left(\frac{h_v}{H}\right)^2 (U_o - U_v)^2}{b} + \left(\frac{h_o}{H}\right)K_o + \left(\frac{h_v}{H}\right)K_v$
Exchange coefficient	$b^{-1} \simeq \frac{h_2^2}{D_w} + \frac{h_1}{k} + \frac{h_1^2}{\left[\frac{1}{h_1}\int_{h_2}^{H} D_z dz\right]}$	$b^{-1} \simeq \frac{h_v^2}{D_w} + \frac{h_o}{k} + \frac{h_o^2}{\left[\frac{1}{h_o}\int_{h_v}^{H} D_z dz\right]}$

show that vortex-driven exchange may be described by an exchange velocity $k = \Delta U / 40$, so that in this limit of behavior

$$b = \frac{\Delta U}{40 h_v} \tag{4.3}$$

Furthermore, with the same manner of Murphy et al. (2007), this study assumes that the difference in layer velocities, $U_o - U_v$, is a constant fraction, α_1, of the total velocity difference, ΔU, i.e.

$$(U_o - U_v) = \alpha_1 \Delta U \tag{4.4}$$

Previous studies of Ghisalberti and Nepf (2005) suggest that $\overline{u'w'} \sim (\Delta U)^2$, so that it is reasonable to assume $\alpha_2 = \Delta U / u_*$ is approximately constant. The exchange term (Eq. (4.2)) is then simplified by substitution of Eq.s (4.3), (4.4), and $\alpha_2 = \Delta U / u_*$. Based on the dispersion observed in emergent canopies (Nepf et al., 1997; White and Nepf, 2003), the term containing K_v is expected to be small compared to the other terms, and is neglected for simplicity. Finally, the dispersion term of overflow (K_o) is derived in section 4.2. For convenience, combining the constants $40\alpha_1^2\alpha_2 = \alpha$, Eq. (4.1) gives

$$\begin{aligned} K_{sf} &= 40\alpha_1^2\alpha_2 \left(\frac{h_o}{H}\right)^2 \left(\frac{h_v}{H}\right)^2 h_v u_* + \left(\frac{h_o}{H}\right) K_o \\ &= \alpha \left(\frac{h_o}{H}\right)^2 \left(\frac{h_v}{H}\right)^2 h_v u_* + \left(\frac{h_o}{H}\right) K_o \end{aligned} \tag{4.5}$$

4.1.2 Diffusion-limited exchange

In dense canopies, $z_1 / h_v \approx 1$ and vortex penetration is limited. With these conditions the in-canopy diffusion controls exchange between the canopy and overflow. When $z_1 = h_v$, Eq. (4.2) reduces to

$$b \cong \frac{D_w}{h_v^2} \tag{4.6}$$

Assuming that the wake-zone diffusivity, D_w, approximates the value observed in emergent canopies, and Substitution of Eq. (4.6) and the relationship observed in field canopies (Lightbody and Nepf, 2006),

$$D_w = 0.17 U_v d \tag{4.7}$$

into Eq. (4.1) and applying similar simplifications to those in section 4.1.1,

$$K_{sf} = \frac{(U_o - U_v)^2}{0.17 U_v}\left(\frac{h_v}{H}\right)^2\left(\frac{h_o}{H}\right)^2\left(\frac{h_v}{d}\right) + \left(\frac{h_o}{H}\right)K_o \tag{4.8}$$

Because vegetative drag is the dominant resistance for $d^2 N \geq 0.01$ (Nepf, 1999), the depth-averaged force balance for steady conditions can be written

$$\rho g S H \approx \frac{1}{2}\rho C_D d N h U_v^2 \tag{4.9}$$

Then, using $u_{*H} = \sqrt{gSH}$ to simplify the left-hand side of Eq. (4.9),

$$\frac{u_*}{U_v} = \left(\frac{C_D dNh_v}{2} \right)^{1/2} \tag{4.10}$$

Substitution of Eq. (4.10) into Eq. (4.8) yields

$$K_{\mathrm{sf}} = \zeta \left(\frac{h_v}{H} \right)^2 \left(\frac{h_o}{H} \right)^2 \left(\frac{h_v}{d} \right) \left(C_D dNh_v \right)^{1/2} + \left(\frac{h_o}{H} \right) K_o \tag{4.11}$$

where the coefficient $\zeta = 4.2[(U_o - U_v) / u_{*H}]^2$.

4.2 Determination of longitudinal dispersion coefficient

The 3D advection-diffusion equation for the unidirectional flow can be written as

$$\frac{\partial C}{\partial t} + \frac{\partial UC}{\partial x} + \frac{\partial VC}{\partial x} + \frac{\partial WC}{\partial z} = \left[\frac{\partial}{\partial x} \left(D \frac{\partial C}{\partial x} \right) + \frac{\partial}{\partial y} \left(D \frac{\partial C}{\partial y} \right) + \frac{\partial}{\partial z} \left(D \frac{\partial C}{\partial z} \right) \right] \tag{4.12}$$

where all the quantities are instantaneous; C = concentration of pollutants; D = diffusivity; and U, V, and W = instantaneous velocities in the longitudinal (x), lateral (y), and vertical (z) directions. Because advection in the flow direction is greater than diffusion, the diffusion term can be neglected and this study considers x-z plane. Moreover, splitting the quantities C, U, and W into vortex-period-averaged quantities and fluctuations over them as

$$C = \langle C \rangle + c', \quad U = \langle U \rangle + u', \quad W = w' \tag{4.13}$$

where the bracketed quantities are time-averaged and small letters with primes are fluctuating quantities. Substituting Eq. (4.13) into Eq. (4.12) and averaging over a vortex-period results in

$$\frac{\partial \langle C \rangle}{\partial t} + \langle U \rangle \frac{\partial \langle C \rangle}{\partial x} = D \frac{\partial}{\partial z} \frac{\partial \langle C \rangle}{\partial z} + \frac{\partial \langle -w'c' \rangle}{\partial z} \tag{4.14}$$

where there is no average velocity in the *z*-direction. The vortex-period-averaged diffusion coefficient can now be defined analogous to turbulent diffusion coefficient as

$$\langle -w'c' \rangle = D_v \frac{\partial \langle C \rangle}{\partial z} \tag{4.15}$$

Substituting Eq. (4.15) into Eq. (4.14) results in

$$\frac{\partial \langle C \rangle}{\partial t} + \langle U \rangle \frac{\partial \langle C \rangle}{\partial x} = \langle D \rangle \frac{\partial^2 \langle C \rangle}{\partial z^2} \tag{4.16}$$

where $\langle D \rangle = D + D_v$ = time and vortex-period-averaged turbulent diffusion coefficient. For brevity, the brackets that denote vortex-period-averaged quantities are omitted henceforth. Further, to average flow depth, the *C* and *U* in Eq. (4.16) are divided into depth-averaged quantities and fluctuating quantities over the depth-averaged. Thus, Eq. (4.16) is written as

$$\frac{\partial\left(\bar{C}+C'\right)}{\partial t}+\left(\bar{U}+U'\right)\frac{\partial\left(\bar{C}+C'\right)}{\partial x}=D\frac{\partial^2 C'}{\partial z^2} \tag{4.17}$$

where quantities with overbars are depth-averaged and those with primes are fluctuations. Changing the time and space coordinate into moving coordinate system (τ , ξ), Eq. (4.17) can be rewritten as

$$\frac{\partial\bar{C}}{\partial\tau}+\frac{\partial C'}{\partial\tau}+U'\frac{\partial\bar{C}}{\partial\xi}+U'\frac{\partial C'}{\partial\xi}=D\frac{\partial^2 C'}{\partial z^2} \tag{4.18}$$

Averaging Eq. (4.18) over depth

$$\frac{\partial\bar{C}}{\partial\tau}+\overline{U'\frac{\partial C'}{\partial\xi}}=0 \tag{4.19}$$

Subtracting Eq. (4.19) from Eq. (4.18)

$$\frac{\partial C'}{\partial\tau}+U'\frac{\partial\bar{C}}{\partial\xi}+U'\frac{\partial C'}{\partial\xi}-\overline{U'\frac{\partial C'}{\partial\xi}}=D\frac{\partial^2 C'}{\partial z^2} \tag{4.20}$$

In Eq. (4.20), As C' is much smaller than $\bar{C}$, the third and fourth terms balance each other and are much smaller than the second term. Thus, Eq. (4.20) can be written as

$$\frac{\partial C'}{\partial\tau}+U'\frac{\partial\bar{C}}{\partial\xi}=D\frac{\partial^2 C'}{\partial z^2} \tag{4.21}$$

After a long time, the solution of Eq. (4.21) is the solution of the steady state form of Eq. (4.21), i.e.

$$U'\frac{\partial\bar{C}}{\partial\xi}=D\frac{\partial^2 C'}{\partial z^2}\qquad\text{with }\frac{\partial C'}{\partial z}=0\quad\text{at } z=0,\ h \tag{4.22}$$

Solution of Eq. (4.22) becomes

$$C'(z) = \frac{1}{D}\frac{\partial \overline{C}}{\partial x}\int_0^z \int_0^z U'dzdz + C'(0) \tag{4.23}$$

The rate of mass transport can now be written as

$$M = \int_0^h U'C'dz = \frac{1}{D}\frac{\partial \overline{C}}{\partial x}\int_0^h U' \int_0^z \int_0^z U'dzdzdz + \int_0^h U'C'(0)dz \tag{4.24}$$

In Eq. (4.24), $\int_0^h U'C'(0)dz = 0$, because $\int_0^h U'dz = 0$. The rate of mass transport can also be given as

$$M = -hK_{wx}\frac{\partial \overline{C}}{\partial x} \tag{4.25}$$

Eq. (4.25) follows Fickian law which states that the flux of the pollutants crossing a unit area per unit time is proportional to the gradient of the solute concentration, and is valid after a sufficiently long time after which the spread of pollutants follows a normal distribution. K_{wx} is the longitudinal dispersion coefficient in wave-current flow. Equating Eq. (4.24) and Eq. (4.25) provides

$$K_{wx} = -\frac{1}{hD}\int_0^h U' \int_0^z \int_0^z U'dzdzdz \tag{4.26}$$

As the quantities on the right side are period-averaged already, the above expression may be rewritten as

$$K_{wx} = \overline{K_x} = -\frac{1}{DT}\int_0^T \frac{1}{h}\int_0^h U' \int_0^z \int_0^z U'dzdzdzdt \tag{4.27}$$

Note that the effective depth of flow was taken to integrate over the depth. If the velocity is time dependent, the dispersion coefficient will also be time

dependent. In the presence of short period waves and steady current, unsteady velocity may be written as

$$U(x,z,t) = U_c(x,z) + U_w(x,z,t) \tag{4.28}$$

where U_c = steady current velocity and U_w = first-order wave-induced velocity that causes the water particles to move faster under a wave crest and slower under trough. A net forward movement thus results. The depth and period-average velocity is given by

$$U(x) = \frac{1}{Th(x)} \int_0^T \int_0^h \left[U_c(x,z) + U_w(x,z,t) \right] dzdt \tag{4.29}$$

Subtracting Eq. (4.29) from Eq. (4.28), the fluctuating velocity component can be expressed as

$$U'(x,z) = U_c'(x,z) + U_w'(x,z,t) \tag{4.30}$$

where U_c' = lateral deviation of the steady current velocity from the depth-averaged steady current velocity; U_w' = lateral deviation of the wave-induced velocity from its time-averaged mean velocity. Assuming constant vertical diffusivity, the final form of wave-current longitudinal dispersion coefficient for overflow region is given by

$$K_{xo} = -\frac{1}{h_o D}\int_0^h \left(U'_{oc} + U'_{ow}\right)\int_0^z \int_0^z \left(U'_{oc} + U'_{ow}\right) dzdzdz$$
$$= -\frac{I_o}{D} \tag{4.31}$$

where T = wave period and I = shear term that is calculated using a combined stream function that is derived in the previous section.

Substituting Eq. (3.28) into Eq. (4.29) with Eq. (4.30) gives

$$U'_o = U'_{oc} + U'_{ow} = \frac{u_*}{\kappa}\left(\log\frac{z_o}{h_o} + 1\right) + k\beta_1 \cosh(kz_o)\cos(kx - \sigma t) \tag{4.32}$$

and the shear term of Eq. (4.31) becomes

$$I_o = \frac{1}{h_o}\int_0^h \left(U'_{oc} + U'_{ow}\right)\int_0^z \int_0^z \left(U'_{oc} + U'_{ow}\right) dzdzdz$$
$$= \frac{1}{h_o}\int_0^h \left(U'_{oc} + U'_{ow}\right)\left[\frac{u_* z_0^2}{4\kappa}\left(2\log\frac{z_0}{h_o} - 1\right) + \frac{\beta_1}{k}\cos\left(kx - \sigma t\right)\left(\cosh(kz_0) - 1\right)\right] dz$$
$$= -\frac{2u_*^2 h_o^2}{27\kappa^2} + \frac{\beta_1^2}{2kh_o}\cos^2\left(kx - \sigma t\right)\left\{\cosh(kh_o)\sinh(kh_o) + kh_o - 2\sinh(kh_o)\right\} \tag{4.33}$$

where U'_{oc} =current only component; and U'_{ow} = first-order wave component. The cross covariances of current with wave will vanish under integral. Substitution of Eq. (4.33) into Eq. (4.31) is K_o of Eqs. (4.5) and (4.11) and divide through by $u_{*H}H$, obtaining the following non-dimensional coefficient of longitudinal dispersion.

$$\frac{K_{sf}}{u_* H} = \alpha \left(\frac{h_v}{H} \right)^3 \left(\frac{h_o}{H} \right)^{5/2} + \left(\frac{h_o}{H} \right)^{3/2} \left[\left(\frac{2}{27\kappa^2 \alpha_2} \right) \left(\frac{h_o}{t_{ml}} \right) + \left(\frac{k \cdot t_{ml}}{2\sinh^2(kh_o)} \right) \left(\frac{a}{H} \right) \left(\frac{\beta_1}{\alpha_2} \right) \right] \tag{4.34a}$$

$$\frac{K_{sf}}{u_* H} = \alpha \left(\frac{h_v}{H} \right)^3 \left(\frac{h_o}{H} \right)^{5/2} + \left(\frac{h_o}{H} \right)^{3/2} \left\{ \cos^2 \left(kx - 2\pi \frac{t}{T} \right) \right\} \times \left[\left(\frac{2}{27\kappa^2 \alpha_2} \right) \left(\frac{h_o}{t_{ml}} \right) + \left(\frac{k \cdot t_{ml}}{2\sinh^2(kh_o)} \right) \left(\frac{a}{H} \right) \left(\frac{\beta_1}{\alpha_2} \right) \right] \tag{4.34b}$$

Eq. (4.34*a*) is period averaged LDC and Eq. (4.34*b*) is unsteady LDC.

5. Results and Conclusion

5.1 Results

As shown in Figure 5.1, for low values of H / h (< 2.5), overflow zone shear plays a significant role on longitudinal mixing. The normalized dispersion of the exchange term peaks at around $H / h = 1.8$, contributing increase of LDC. Conversely, as H / h increases, logarithmic shear dispersion in the overflow zone grows and exchange is not influential (negligible for $H / h > 5$ as expected). Over the range $H / h > 3$, dimensionless longitudinal dispersion coefficient asymptotes to the value of LDC without consideration of vegetation. Comparing to total LDC of K_{ss}, K_{sf} widens a gap to almost 25% at $2 < H / h < 3$. This result is related from the effect of wave although the absolute value of wave term is extremely small. That's because the current term is induced from the wave-current flow, even so excluding the exchange term (Figure 5.2), and current term of K_{sf} is larger than that of K_{ss} as almost same as the difference between the total values.

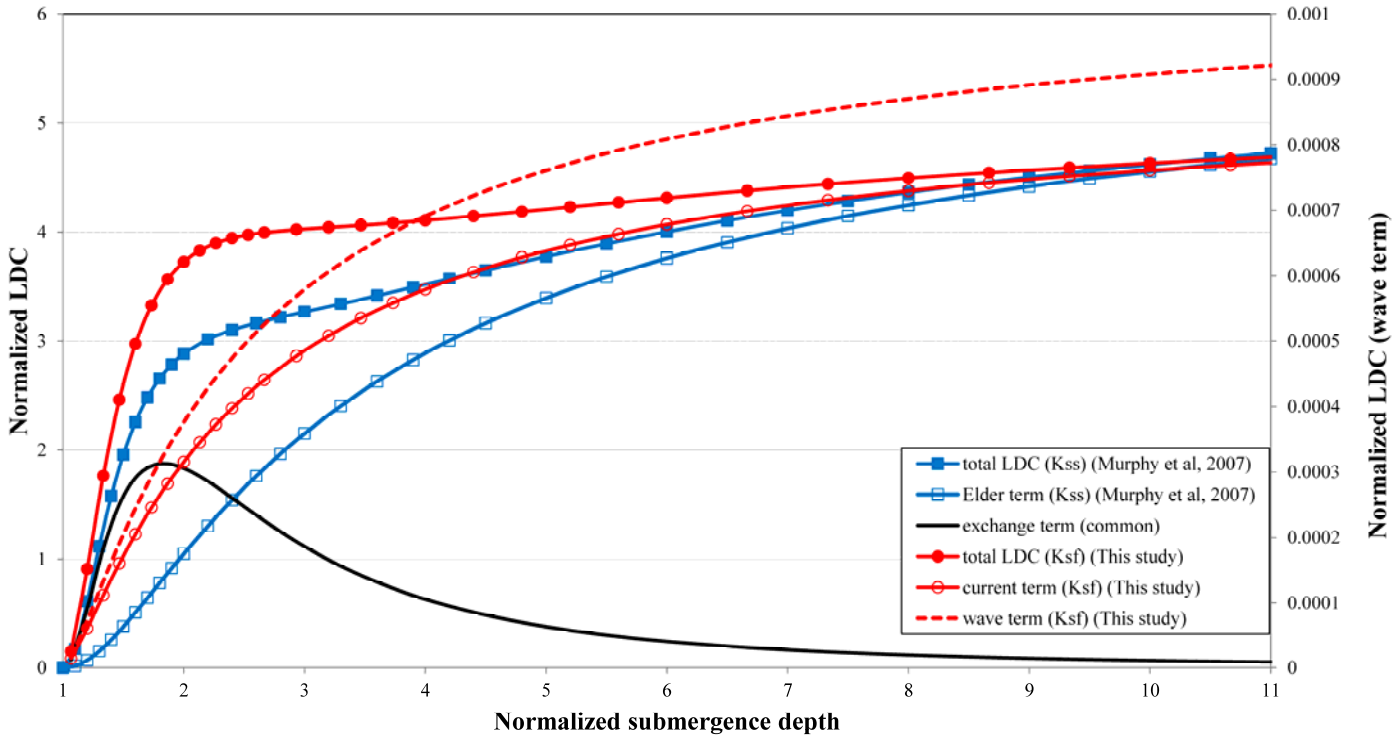

Figure 5.1 Contributions of each term to dispersion coefficient

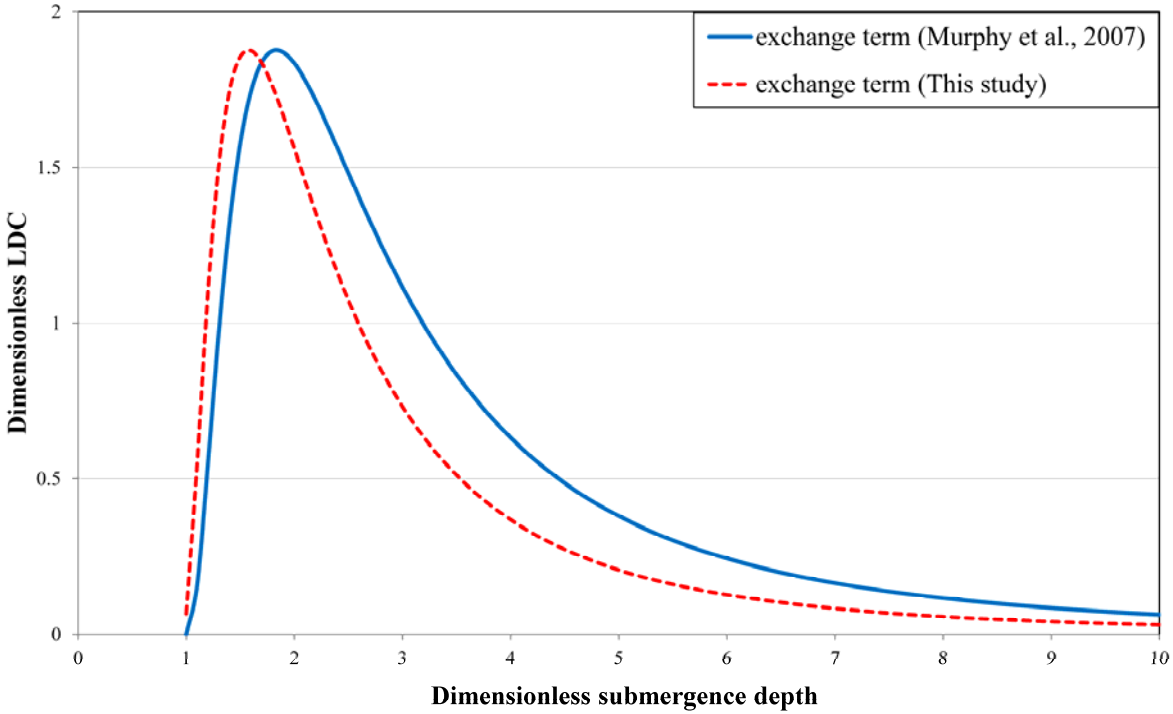

Figure 5.2 Difference of each exchange terms

When pollutants in laminar or turbulent flow are transported, and mixing spread them over the flow, after which the balance between longitudinal shear and vertical diffusion leads to the Gaussian distribution of the pollutants along the channel. In non-oscillatory flows such as in open channels or pipes, the time required by pollutants to reach to this phase is h^2 / D, [h = flow depth, and D = molecular diffusivity (turbulent diffusivity for turbulent flow)], whereas in oscillatory flows the steady state phase reaches when the mixing time $T_c = h^2 / D$ is much higher than the wave period (T), i.e., $T / T_c \rightarrow \infty$. Before the steady state phase, mixing is dominated by the momentum of pollutants and is called the initial unsteady phase of mixing (Fischer et al. (1979)).

As shown in Figure 5.3, the amplitude of oscillation in apparent dispersion coefficient increases initially up to a certain extent of time and then becomes stable for a long time. However, the above situation stabilizes after a time in which the solute disperses at a fairly uniform rate with steady oscillation of constant amplitude. If considering velocity profiles – steady and time-dependent part separately – the steady part shows a more significant role at large time on the LDC than the periodic part. This means for long period

(a) Long period wave ($T / T_c = 10$ (i.e., $\rightarrow \infty$))

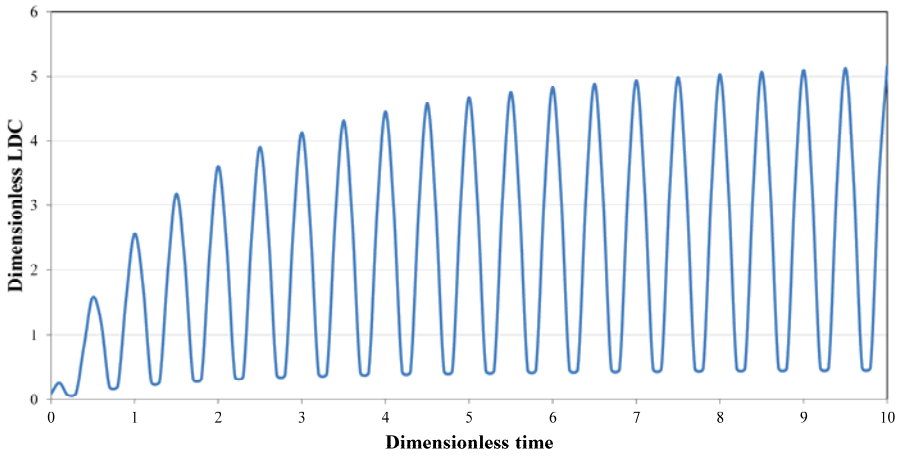

(b) Short period wave ($T / T_c = 0.01$ (i.e., $\rightarrow 0$))

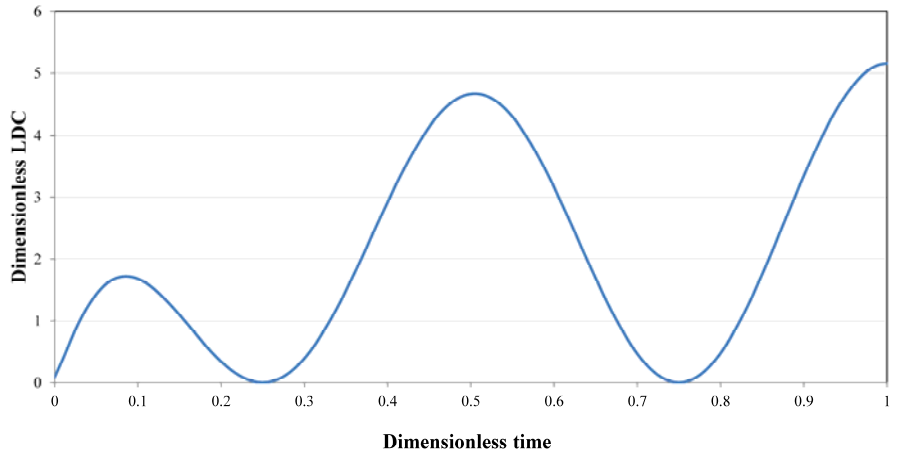

Figure 5.3 Variation of the LDC for two extremities

wave, the concentration can adopt the velocity profile of itself. Therefore the LDC will be the same as if flow were steady except during a short period. For opposite extremity, when period is very short compared to mixing time, the solute can be expected to oscillate and the LDC tends to be zero.

5.2 Conclusion

The study conducts derivation and investigation a theoretical solution of the combined wave-current flow through submerged vegetation. In the case of submerged vegetation, a depthwise logarithmic velocity profile is assumed to simulate the current in the overflow region with a virtual bottom boundary near the interface which becomes depthwise constant in the vegetation region.

To induce the wave element, small-amplitude monochromatic waves are assumed and using a linear wave theory, the wave components to the first order are derived for both of the velocities. Thus, the proposed mathematical model consists of a rotational wave-current flow in the overflow layer and a constant current in the vegetation layer with an irrotational wave-induced flow. Combined wave-current-vegetation flow derives the mathematical model in

which stream functions for combined flows are derived separately for overflow and vegetation regions and then coupled to obtain expressions for interfacial wave.

These velocity profiles from the series of procedures are utilized to determine the longitudinal dispersion coefficient. Its method stems from Two-box model of Murphy et al. (2007) and is adopted with some modification. Derived solution for the longitudinal dispersion coefficient is composed of the longitudinal dispersion terms in each layer. For the vegetation layer, the longitudinal dispersion term is assumed equivalent to the dispersion coefficient in an emergent canopy and it can be negligible due to stem-scale contributions to dispersion. For larger submergence depth the LDC asymptotes to the value without consideration of vegetation of Elder's simple analytical expression. Differences between total LDC of K_{ss} and K_{sf} is almost 25% at relatively small submergence depth. This result is related from the effect of wave only distinction between two cases in spite of extremely small value.

The knowledge deduced theoretically and obtained by completing idealized equation with many assumptions only helps to understand processes

rather than delivers a final result – this knowledge explains how processes evolve, but is incapable to predict what actually happens in the nature. Obviously the further progress can be achieved by performing field experimental studies which will bring together the theoretical grounds, the reality of nature, and a certain control of the variables which is essential of any experimentation.

Available theories of transport processes and mixing in the fluvial systems provide possibilities for describing the effect of vegetation through the dead zone parameters. However, presently there is a lack of knowledge on the mechanisms of dead zone formation by the vegetation patches which can be only comprehended through the knowledge of details on the structure and dynamics of turbulent flow around and within the vegetation patches.

6. Reference

Ackerman, J. D. and Okubo, A. (1993). Reduced mixing in a marine macrophyte canopy. *Funct Ecol*, 7(3), 305-309.

Aeschlimann, V., Prothin, S., Barre, S., and Djeridi, H. (2012). High speed visualizations of the cavitating vortices of 2D mixing layer. *Eur J Mech B-Fluid*, 31, 171-180.

Anh, T. L. (2011). Pollutant transport in constructed subsurface flow wetlands, Lambert Academic Publishing.

Baddour, R. E., and Song, S. W. (1998). The rotational flow of finite amplitude periodic water waves on shear currents. *Appl Ocean Res*, 20(3), 163-171.

Baptist, M. J., Babovic, V., Uthurburu, J. R., Keijzer, M., Uittenbogaard, R. E., Mynett, A., and Verwey, A. (2007). On inducing equations for vegetation resistance. *J Hydraul Res*, 45(4), 435-450.

Chikwendu, S. C. (1986). Calculation of longitudinal shear dispersivity using an N-zone model as $N \rightarrow$ infinity. *J Fluid Mech*, 167, 19-30.

Chikwendu, S. C., and Ojiakor, G. U. (1985). Slow-zone model for longitudinal dispersion in two-dimensional shear flows. *J Fluid Mech*, 152(Mar), 15-38.

Dean, R. G., and Dalrymple, R. G. D. R. A. (1991). *Water wave mechanics for engineers & scientists*, World Scientific.

Deng, Z. Q., Singh, V. P., and Bengtsson, L. (2001). Longitudinal dispersion coefficient in straight rivers. *J Hydraul Eng-ASCE*, 127(11), 919-927.

Dijkstra, J. T., and Uittenbogaard, R. E. (2006). Modelling hydrodynamics in flexible vegetation. *Physical Processes in Natural Waters Workshop* (Sept 4-7), Lancaster, England.

Elder, J. W. (1959). The dispersion of marked fluid in turbulent shear flow. *J Fluid Mech*, 5(4), 544-560.

Finnigan, J. (2000). Turbulence in plant canopies. *Annual Review of Fluid Mechanics*, 32, 519-571.

Finnigan, J. J., and Mulhearn, P. J. (1978). Modeling waving crops in a wind tunnel. *Boundary-Layer Meteorol*, 14(2), 253-277.

Fischer, H. B. (1973). Longitudinal dispersion and turbulent mixing in open-channel flow. *Annual Review of Fluid Mechanics*, 5, 59-78.

Fischer, H. B. (1979). *Mixing in inland and coastal waters*, Academic Press.

Fitzmaurice, L., Shaw, R., Paw U, K., and Patton, E. (2004). Three-dimensional scalar microfront systems in a large-eddy simulation of vegetation canopy flow. *Boundary-Layer Meteorol*, 112(1), 107-127.

Gayev, Y. A., and Hunt, J. C. R. (2006). Flow and transport processes with complex obstructions: applications to cities, Vegetative Canopies and Industry, Springer.

Ghisalberti, M., and Nepf, H. M. (2002). Mixing layers and coherent structures in vegetated aquatic flows. *J Geophys Res-Oceans*, 107(C2).

Ghisalberti, M., and Nepf, H. M. (2005). Mass transport in vegetated shear flows. *Environ Fluid Mech*, 5(6), 527-551.

Huthoff, F. (2007). Modeling hydraulic resistance of floodplain vegetation, University of Twente.

Klopstra, D., Barneveld, H. J., Noortwijk, J. M., and Van Velzen, E. H. (1997). Analytical model for hydraulic roughness of submerged vegetation. *Proceedings of the 27th International Association for Hydraulic Research Congress theme A Managing Water: Coping with Scarcity and Abundance, San Fransisco*, 775-780.

Kundu, P. K., and Cohen, I. M. (2002). *Fluid Mechanics*, Academic Press.

Lee, Y. G., and Kim, J. W. (2005). *Riparian vegetation of South Korea*, Keimyung University Press

Lightbody, A. F., and Nepf, H. M. (2006). Prediction of velocity profiles and longitudinal dispersion in emergent salt marsh vegetation. *Limnol Oceanogr*, 51(1), 218-228.

Murphy, E., Ghisalberti, M., and Nepf, H. (2007). Model and laboratory study of dispersion in flows with submerged vegetation. *Water Resour Res*, 43(5).

Nepf, H. M. (1999). Drag, turbulence, and diffusion in flow through emergent vegetation. *Water Resour Res*, 35(2), 479-489.

Nepf, H. M. (2012). Flow and transport in regions with aquatic vegetation. *Annu Rev Fluid Mech*, 44, 123-142.

Nepf, H. M., Mugnier, C. G., and Zavistoski, R. A. (1997). The effects of vegetation on longitudinal dispersion. *Estuar Coast Shelfs*, 44(6), 675-684.

Nepf, H. M., and Vivoni, E. R. (2000). Flow structure in depth-limited, vegetated flow. *J Geophys Res-Oceans*, 105(C12), 28547-28557.

Nezu, I., Nakagawa, H., and Research, I. A. f. H. (1993). *Turbulence in open channel flows*, Taylor & Francis Group.

Petryk, S., and Bosmajian, G. (1975). Analysis of flow through vegetation. *J Hydr Eng Div-ASCE*, 101(7), 871-884.

Poggi, D., Porporato, A., Ridolfi, L., Albertson, J. D., and Katul, G. G. (2004). The effect of vegetation density on canopy sub-layer turbulence. *Boundary-Layer Meteorol*, 111(3), 565-587.

Polatel, C. (2006). Large-scale roughness effect on free-surface and bulk flow characteristics in open-channel flows. *PhD diss.,University of Iowa*.

Raupach, M. R., Finnigan, J. J., and Brunet, Y. (1996). Coherent eddies and turbulence in vegetation canopies: The mixing-layer analogy. *Boundary-Layer Meteorol*, 78(3-4), 351-382.

Rutherford, J. C. (1994). *River mixing*, Wiley.

Seo, I. W. (1990). Laboratory and numerical investigation of longitudinal dispersion in open channels. *Water Resour Bull*, 26(5), 811-822.

Seo, I. W., and Baek, K. O. (2004). Estimation of the longitudinal dispersion coefficient using the velocity profile in natural streams. *J Hydraul Eng-ASCE*, 130(3), 227-236.

Seo, I. W., and Cheong, T. S. (1998). Predicting longitudinal dispersion coefficient in natural streams. *J Hydraul Eng-ASCE*, 124(1), 25-32.

Stone, B. M., and Shen, H. T. (2002). Hydraulic resistance of flow in channels with cylindrical roughness. *J Hydraul Eng-ASCE*, 128(5), 500-506.

Sun, X. (2009). Flow characteristics in vegetated compound channels: vegetation, experiment, modeling, VDM Publishing.

Taylor, G. (1953). Dispersion of soluble matter in solvent flowing slowly through a tube. *Proc R Soc Lon Ser-A*, 219(1137), 186-203.

White, B. L., and Nepf, H. M. (2003). Scalar transport in random cylinder arrays at moderate Reynolds number. *J Fluid Mech.*, 487, 43-79.

Yang, W., and Choi, S.-U. (2010). A two-layer approach for depth-limited open-channel flows with submerged vegetation. *J Hydraul Res.*, 48(4), 466-475.

국문초록

침수식생이 있는 2차원 흐름에서의 종방향 분산계수 산정

서울대학교 대학원
건설환경공학부
박 선 영

수변 환경에서 식생은 하천의 흐름특성과 오염물질의 혼합특성을 결정짓는 중요한 역할을 한다. 본 연구에서는 식생이 있는 흐름의 혼합특성을 파악하기 위해 2차원 이송-분산 방정식의 종방향 분산계수에 연구의 초점을 맞추었다. 종분산계수에 영향을 미치는 인자를 흐름방향 유속의 수심방향 분포특성으로 한정하여 유연한 식생이 물 속에 잠겨있는 상태의 흐름에서 유속 분포식을 이론적으로 유도하였고 이를 종분산계수식에 이용하였다.

식생층과 표층이 흐름을 달리함에 따라 층간 경계면에서는 유속분포에 변곡점이 발생하고 Kelvin-Helmholtz (K-H) 불안정성이 진행파를 만든다. 본 연구에서는 식생의 유연도가 이 파랑을 온전히 나타낸다는 가정하에 유연한 식생의 물리적 효과를 파와 흐름을 결합한 유동함수로 표현하였다. 파와 흐름, 그리고 식생이 결합된 수직 2차원 비압축성 유체에 대해 유동함수는 식생층과 표층으로 각각 유도하였고 경계면에서 연직방향 유속을 같게 정합시켰다. 표층의 흐름부분은 정상상태의 로그유속분포를 기반으로 하고 식생층의 흐름부분은 깊이방향으로 일정한 유속을 설정하였다.

각 층의 유동함수에서 유도된 파와 흐름이 결합된 유속분포식으로부터 본 연구에서는 Murphy 등 (2007)이 제안한 two-box 모형을 본 연구에 맞게 수정하여 식생이 있는 2차원 흐름에서의 종방향 분산계수 식을 산정하였다. 무차원 종분산계수를 잠몰깊이 변화에 따라 살펴본 결과, 상대적으로 큰 잠몰깊이 (H / h > 5)에 대해서는 식생이 없는 흐름에서의 종분산계수 값에 점근하였다. 작은 잠몰깊이에 대해서는 식생의 유연성을 고려하지 않은 Murphy 등 (2007)의 모형의 값과 최대 약 25% 큰 값을 나타냈다. 종분산계수를 구성하고 있는 부분에 대하여 각각 그 기여도를

고려해보면 파랑 부분과 경계면에서의 교환에 의한 부분은 기존의 연구 결과와 큰 차이를 보이고 있지 않으나 파랑이 결합되면 파랑의 효과가 종분산계수의 차이를 만들어냄을 알 수 있었다. 이는 유연한 식생의 경계층에서 생긴 파(monami)가 오염물질이 식생층으로 침투하는 정도를 증진시킴으로써 혼합효과를 높이고 있다는 것을 의미하며 충분한 혼합시간을 가질 수 있는 장주기파가 발생할 때는 흐름의 정상상태 부분이 더욱 중요한 역할을 함을 확인하였다.

주요어: 침수식생, 식생유연도, 종분산계수, K-H 불안정성, monami, two-box 모형

학번: 2011-20975

감사의 글

졸업을 앞두고 논문을 마무리하며 지난 2 년을 되돌아 보니, 학문적인 배움 그 이상의 값진 것들을 많이 얻은 것 같습니다. 먼저, 연구방향에 대한 넓은 안목과 아낌없는 조언으로 소중한 가르침을 베풀어주신 서일원교수님, 김영한선생님, 이길성교수님, 서경덕교수님, 김영오교수님, Van Thinh Nguyen 교수님께 깊은 감사의 마음을 전하고 싶습니다. 특히, 따뜻한 관심과 애정 어린 질책으로 저를 일깨워주시고 독려해주신 지도교수 서일원교수님, 제가 하고 싶은 연구할 수 있도록 배려해주셔서 진심으로 감사 드립니다.

수공학연구실 모든 동기, 선후배님들께도 고마운 마음을 표하고 싶습니다. 특히, 환경수리학연구실 식구들, 정말 고맙습니다. 고되고 긴 여정, 같은 곳을 바라보고 함께 걷는다는 것만으로도 든든한데 부족한 저의 모습까지도 보듬어주고 제가 끈을 놓지 않을 수 있도록 보내준 응원 잊지 않겠습니다. 가장 가까이서 배우고 느낀 모든 것들은 그 어디에서도 얻지 못할 소중한 것들이라고 생각합니다. 제가 받은 사랑만큼 베풀면서 살 수 있는 사람이 되어 보답하겠습니다.

지난 2년은... 나는 누구인가 무엇에 자신 있고 무엇이 부족하며, 무엇을 좋아하고 원하는지, 원하는 것을 이루기 위해 어떤 노력을 얼마나 할 수 있는지 등의 물음들에 답을 얻어가는 시간이었습니다. 환경수리학연구실에서 보낸 시간은 그 어떤 도전 앞에서도 제게 큰 용기와 힘을 줄 것입니다. 졸업을 하면 제 꿈을 위해 또 다시 한 발을 내딛게 되겠지요. 꿈의 결실이 맺어질 때까지 많은 분들의 도움이 헛되지 않도록 겸손한 자세로 중심 잡고 묵묵히 나아가겠습니다.

누구보다 큰 힘이 되어주시는 부모님이 있었기에 제가 늘, 더 큰 꿈을 가지고 살아갈 수 있었습니다. 언제나 저의 길을 믿고 지원해주신 부모님, 감사하고 사랑합니다. 또한, 믿음직스런 모습과 진취적이고 긍정적인 생각으로, 저를 이끌어주는 하나뿐인 동생, 찬희에게도 고마움을 전합니다. 끝으로 이 모든 것들을 허락하신 하나님께 감사 드립니다.

2013년 눈이 유독 많이 왔던 겨울, 그 끝자락에서...